THESIS FOR THE DEGREE OF THE DOCTOR OF PHILOSOPHY

Lipid Nanotubes as a Model for Highly Curved Cellular Membrane Structures

NATALIA STEPANYANTS

Department of Chemical and Biological Engineering
CHALMERS UNIVERSITY OF TECHNOLOGY
Göteborg, Sweden 2013

Lipid Nanotubes as a Model for Highly Curved Cellular Membrane Structures

NATALIA STEPANYANTS

Department of Chemical and Biological Engineering
Chalmers University of Technology
SE-412-96 Göteborg
Sweden
Phone +46 (0) 31 772 1000

Lipid Nanotubes as a Model for Highly Curved Cellular Membrane Structures

NATALIA STEPANYANTS
Department of Chemical and Biological Engineering
Chalmers University of Technology

Abstract

Cells and their organelles show a variety of membrane morphologies with multiple submicrometer features, for example, tubules, vesicles, folds and pores. The shape of the cellular membranes can dynamically change to support a variety of functions, such as cargo transport, transmission of signals between the cells, cell movement and division. A convenient route to understanding the complexity of cellular membranes is to study artificially created lipid bilayer membrane systems. The work presented in this thesis is focused on highly curved membrane structures in the form of lipid bilayer nanotubes.

Firstly, the shape transformation mechanism for free floating lipid nanotubes was investigated. Driven by their high curvature energy, nanotubes contract in length and eventually transform into tubular stomatocyte-like structures. Secondly, diffusion, electric field and Marangoni-flow-driven modes of transport through lipid nanotubes are described. Then, an important improvement in the characterization of lipid nanotubes was achieved by developing a new technique for the measurement of lipid nanotube radii. This technique is based on monitoring the translocation of a photobleached tube region between two nanotube-connected vesicles during the growth of a receiving/daughter vesicle. The validity of this measurement technique was confirmed using super resolution microscopy. In addition, our technique has proven useful for tracking membrane bending rigidity changes in response to environmental and compositional alterations, both in cell plasma membranes and in model vesicle systems. Finally, a microfluidic pipette with a self-confining volume at the tip was presented. It allows for selectively affecting a chosen cell and accessing membranes on the single cell level.

Keywords

Vesicle, network, lipid nanotube, shape transformation, transport, nanotube radii, bending rigidity, cholesterol, sterol, lipid ion interactions, single cell analysis.

LIST OF PUBLICATIONS

This thesis is based on the work presented in following research papers:

I   **Spontaneous Shape Transformation of Free-Floating Lipid Membrane Nanotubes**

Natalia Stepanyants, Haijiang Zhang, Tatsiana Lobovkina, Paul Dommersnes, Gavin D. M. Jeffries, Aldo Jesorka, Owe Orwar

II   **Generation of Phospholipid Vesicle-Nanotube Networks and Transport of Molecules therein**

Aldo Jesorka, Natalia Stepanyants, Haijiang Zhang, Bahanur Ortmen, Bodil Hakonen, Owe Orwar

III **Radial Sizing of Lipid Nanotubes Using Membrane Displacement Analysis**

Natalia Stepanyants, Gavin D. M. Jeffries, Owe Orwar, Aldo Jesorka

IV   **Studying compositional and environmental effects on the bending rigidity of vesicles and cell plasma membranes using lipid nanotubes**

Natalia Stepanyants, Tuomas Näreoja, Aldo Jesorka, Gavin D. M. Jeffries

V   **A Microfluidic Pipette for Single-Cell Pharmacology**

Alar Ainla, Erik T. Jansson, Natalia Stepanyants, Owe Orwar, Aldo Jesorka

CONTRIBUTION REPORT

Paper I   Designed, performed and analyzed all experiments, interpreted the results and made a major contribution to the writing of the paper.

Paper II   Performed the diffusion transport experiments and contributed to the writing of the paper.

Paper III   Proposed the concept, designed, performed and analyzed all experiments, interpreted the results and made a major contribution to the writing of the paper.

Paper IV   Proposed the concept, designed, performed and analyzed experiments, interpreted the results and made a major contribution to the writing of the paper. The STED experiments were performer together with Tuomas Näreoja.

Paper V   Contributed to the experiments associated with the cell plasma membrane blebs.

ABBREVIATIONS

GUV(s)	giant unilamellar vesicle(s)
NVN(s)	nanotube vesicle network(s)
SPE	soybean lipid polar extract
CMC	critical micellar concentration
CPP	critical packing parameter
SUV(s)	small unilamellar vesicle(s)
LUV(s)	large unilamellar vesicle(s)
MLV	multilamellar vesicle
DIC	differential interference contrast
DTT	dithiothreitol
MβCD	methyl-beta-cyclodextrin
DV	daughter vesicle
STED	stimulated emission depletion

CONTENTS

1   INTRODUCTION

The lipid bilayer is vital for the organization and functioning of cells, their plasma membranes and membrane-enclosed organelles. The typical size of an animal cell is 10-20µm [1], but cellular membranes have a defined structure at an even smaller scale [2]. A lot of cellular membrane structures have complex shapes, coupled to a specific process, and features with characteristic dimensions on the order of tens or hundreds of nanometers [3-4], corresponding to regions of highly positive or negative membrane curvatures. Furthermore, the shapes of the membranes are dynamically changing in the course of cell functioning. Good examples thereof are vesicular-tubular clusters responsible for sorting of cargos at the endoplasmic reticulum-Golgi complex intermediate compartment [5] or long tubular structures of mitochondria, which continuously divide and fuse [3]. Despite extensive studies of the molecular machinery involved in membrane reorganization, there are still many open questions in areas such as docking and fusion of synaptic vesicles [6], formation of tunneling nanotubes between cells [7], mitochondria dynamics [3] and viral fusion [8].

Considering the shape complexity, small size-scale, and constant dynamic reorganization of the membrane structures mentioned above, it is clear that all aspects of cell membrane behavior cannot be addressed using only artificial model systems, like giant unilamellar vesicles (GUVs) [9] or supported lipid bilayers [10], where the lipid bilayer is relatively flat. In this thesis a technique which allows the construction of nanotube vesicle networks (NVNs) [11] has been used to model and improve our understanding of highly curved membranes structures, their behavior and function.

The NVN construction procedure is based on a sequence of micromanipulations of a GUV connected to a lipid reservoir, and provides the ability to control the geometry of the produced structures. This advantage has been used to examine the shape optimization [12-14] of tubular lipid membrane structures and to model the exocytose pore [15]. While most of the membrane shape transformation studies have looked at spherical vesicles under an external influence [16-18], introduction of electrically initiated membrane fusion into NVN systems has enabled the formation of circular nanotubes freely floating in solution [19]. The same technique has been used in Paper I to create long linear freely floating nanotubes, as a means to investigate the mechanism of their spontaneous shape transformation. This study together with another report [20] raises the question whether fundamental membrane properties, such as rates of the interleaflet lipid transport and membrane permeability, could be different in highly curved membranes.

The internal volumes of the vesicles in NVNs closely resemble cells communicating via tunneling nanotubes [21]. The analyte solution injected into each individual vesicle in the network can be controlled, providing a useful tool to study enzymatic reactions in

confined volumes [22-23] or modes of analytes transport through the nanotubes (Paper II). The nanotube radius is an important parameter for all such investigations, but since the radius value lies far below the diffraction limit of optical microscopy, it is challenging to measure it directly. Currently existing techniques, such as electrochemical and coalescence methods, give quite a wide range of values [24-25]. In Paper III, a novel simple approach for the determination of nanotube radii is presented.

Various pathological conditions, such as brain injuries, neurodegenerative diseases [26] or cholesterol deficiency diseases [27] can lead to abnormalities in cell membrane organization and function, preventing the normal operation of cells. In these cases, it is important to separate the effects of the given condition on lipid bilayer properties from the effects of other mechanisms the cells use to remodel their membranes [28]. Lipid bilayer membrane physical properties, in particular bending rigidity, define the membrane's ability to curve and form the desired structures. In Paper IV it is shown that the nanotube radial sizing technique from Paper III is also capable of detecting relative changes in the membrane bending rigidity due to environmental variations or membrane composition modifications.

To bridge the gap between artificial and biological lipid membranes, and directly introduce membrane proteins into the vesicle networks [29-30], a protocol for creating NVNs from cell plasma membranes blebs [31-32] was developed [33]. Consequently, the radial sizing technique can be also applied to examine cell plasma membrane rigidity (Papers III and IV), and potentially be used for single cell studies in combination with microfluidic devices, which are capable of selective exposure of a chosen cell to numerous solutions (Paper V).

2 BIOLOGICAL MEMBRANES AND SIMPLIFIED MODELS THEREOF

The two main components of biological membranes are lipids and proteins. On average, there are around 50 lipid molecules per protein, although the ratio can differ significantly between different types of membranes [1]. Lipids constitute the basic two-dimensional liquid bilayer structure of the membrane, while the proteins are in charge of more specific tasks. Bilayer structures form spontaneously and easily from lipid molecules in a water environment, and artificial membranes, have been used to study fundamental membrane properties, such as membrane permeability [34], lateral [35] and interleaflet [36] mobility of lipids, organization of membrane domains, and phase separation [37].

There is a variety of artificial lipid bilayer systems, which can be used as simple models for biological membranes. The black lipid membrane [38] is the earliest system and is particularly convenient for studying membrane permeability and electric properties, but has a limited lifetime. In contrast, supported lipid bilayers [10] are much more stable and allow the use of a number of surface characterization tools, which is not possible for samples suspended in solution. One of the disadvantages of supported lipid bilayers is the possibility of unwanted interactions with the solid support. The majority of the work in this thesis (Papers I-IV) was performed on spherical lipid bilayer structures called vesicles [9]. The membrane in this system is accessible for manipulations and producing lipid membrane nanotubes. In this chapter, vesicle classification and preparation methods will be described, together with the basic principles for lipid self-assembly, a technique for cell plasma membrane vesiculation and the importance of the single cell approach.

2.1. Self-assembly of phospholipids

Lipids have an amphiphilic nature, meaning that they have both polar (hydrophilic) and nonpolar (hydrophobic) parts (Figure 2.1A). Biological membranes are mainly built from phospholipids. Their hydrophobic part consists of two hydrocarbon tails, normally fatty acids having 14 to 24 carbon atoms with varying degrees of saturation. The hydrophilic part of phospholipids typically contains glycerol, a phosphate group, and a polar or charged organic molecule (e.g. choline, ethanolamine, serine, glycerol or inositol), and then they are called phosphoglycerides (Figure 2.1A-B). The exception is sphingomyelin, which contains sphingosine instead of glycerol. An example of phosphoglyceride with a choline head group and two saturated fatty acid tails sixteen carbon atoms long, 1,2-dipalmitoyl-sn-glycero-3-phosphocholine, is shown in Figure 2.1B. Another important class of lipids is sterols, in
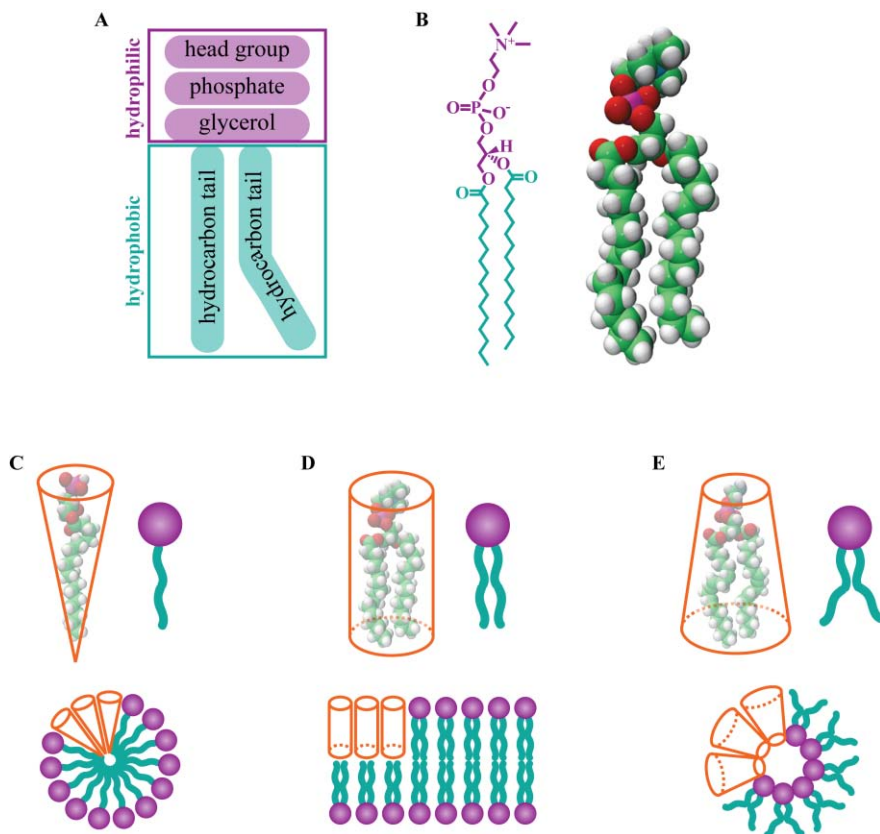
Figure 2.1 Lipid structure and self-assembly. (A) A general structure of the phosphoglyceride molecules, most common lipids of animal cells. (B) The chemical and three-dimensional structure of phosphatidylcholine with two saturated fatty acid chains. (C-E) Illustration of self-assembly into micelles (C), bilayers (D) or inverted micelles (E) according to lipid shape.

particular cholesterol in animal cells. Their influence on the membrane properties will be discussed in Chapter 3. The lipid material used in this thesis (Papers I-IV) is soybean lipid polar extract (SPE). It contains 45.7% of phosphatidylcholine, 22.1% of phosphatidylethanolamine, 18.4% of phosphatidylinositol, 6.9% of phosphatidic acid and 6.9% of unknown components.

At very low concentrations, amphiphilic molecules exist in water environment as monomers. In this case, the polar parts of the molecule have energetically favorable interactions with water, while hydrophobic parts interfere with the surrounding water molecules organization, increasing the entropic energy of the system. After the concentration reaches a certain level, called critical micellar concentration (CMC),

monomers start to form assemblies where hydrophobic parts interact with each other, minimizing the contact with water molecules. CMCs for naturally occurring phospholipids are in the nanomolar range. The energy cost for increasing the order of the amphiphilic molecules is compensated by the removal of the surrounding water organization.

The type of assemblies formed is determined by the geometry of a given lipid molecule (Figure 2.1C-E), described by dimensionless critical packing parameter (CPP) P [39]

$$P = \frac{v}{l \cdot a_0}$$

(2.1)

where a_o is the optimal surface area of the head group, v and l are the effective volume and length of the hydrocarbon chains. If $P < 1/3$ or $1/3 < P < 1/2$, then the lipid shape is a cone or truncated cone, and spherical or tubular micelles are formed (Figure 2.1C). If $1/2 < P \leq 1$, as in case of most phospholipids, then the shape is close to that of a cylinder and bilayers are formed (Figure 2.1D). Lipids with $P > 1$ assemble into inverted micelles (Figure 2.1E). Mixed lipids with different CPPs can form bilayers by compensating each other's shape. When such a bilayer is bent the lipids can favor regions where membrane curvature better accommodates their shape [40]. Micelles, bilayers and inversed micelles can arrange themselves into even higher-ordered structures, forming different lipid phases. Lipid aggregates used in this thesis were in a lamellar liquid-disordered phase, where lipids are organized in two-dimensional liquid bilayers (lamellae) and can diffuse in lateral directions. At low temperatures, the liquid-disordered phase transitions into a liquid-crystalline phase and the lipids lose their lateral mobility.

2.2. Classification of vesicles

Vesicles are spherical lipid assemblies formed when a lipid bilayer self-closes in water solution, trapping part of the solution inside (Figure 2.2A). Vesicles which have only one lipid bilayer wall are called unilamellar vesicles. They are usually classified by their size into small (10-100nm), large (10nm-1µm) and giant (larger than 1µm) unilamellar vesicles. Vesicles can also be oligolamellar; in other words, have several bilayers in their wall (Figure 2.2B, left). Small and large unilamellar vesicles (SUVs and LUVs) are used to form supported lipid bilayers [41] and are, furthermore, frequently used as drug delivery carriers for various pharmaceutical and cosmetic products [42]. GUVs, due to their size, are convenient for light microscopy studies and a number of micromanipulation techniques [11, 43-45]. GUVs are a useful tool for mimicking certain properties of cells [46-47], such as in the examination of membrane mechanical properties [43], organization of membrane domains [48] and rearrangement of the membrane shape by proteins [49].

5

Vesicles where all of the inner volume is filled with bilayers, forming an onion-like structure, are called multilamellar (MLV) (Figure 2.2B, right). In this thesis (Papers I-IV), complexes of GUV connected with MLV (Figure 2.2, center) were used to produce NVNs (Chapter 5). In this arrangement the GUV membrane is accessible for micromanipulations with a glass micropipette, while the MLV provides lipid material for formation of NVN. Bilayers of the MLVs' lamellars are interconnected so that the MLV can unroll when the membrane is pulled from the GUV. It is necessary to note, that oligo- and unilamellar vesicle walls cannot be easily distinguished by light microscopy and additional controls are required to be sure that a given GUV is in fact unilamellar. Until recently, unilamellarity of GUVs was assumed in most of experiments with NVNs, while the results described in Papers III-IV of this thesis show that there is a distribution of lamellarities in vesicle samples, which is specific for each lipid composition, as well as the storage and preparation parameters used. Various approaches to validate vesicle lamellarity will be described further in this chapter.
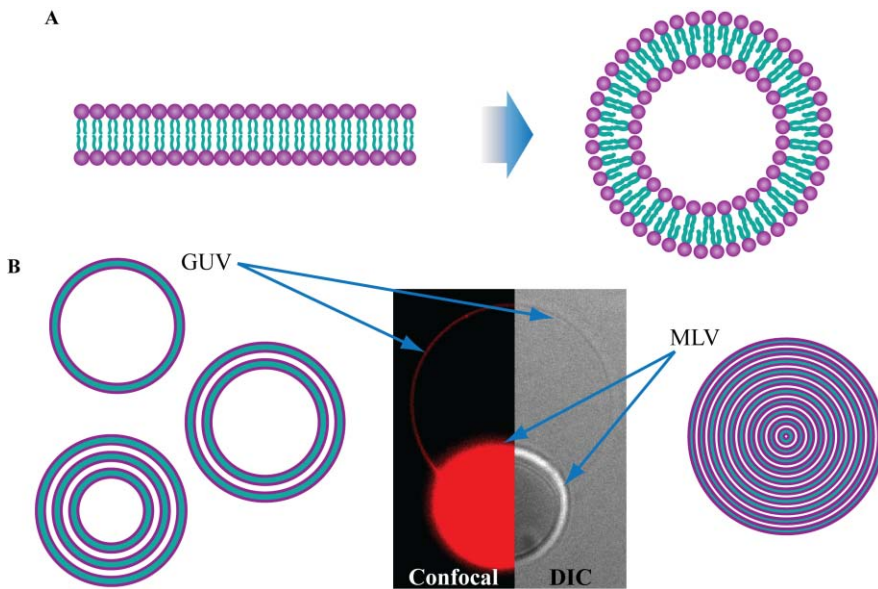
Figure 2.2 Vesicle and their lamellarity. (A) A flat lipid bilayer forms a spherical vesicle to avoid exposing the hydrophobic regions at the edge to water. (B) Shared confocal and DIC image of GUV (~20μm in diameter) attached to MLV. Microscopy imaging cannot easily distinguish vesicles with one or several walls, which is why vesicles referred to as GUVs might in fact contain more than one bilayer (B, left). The MLV has a large number of bilayers (B, right). It appears as a bright object in fluorescence microspore and has a contrast edge in the DIC image.

2.3. Preparation of giant unilamellar vesicles

A number of methods have been used to obtain thin-walled (uni- and oligolamellar) vesicles [9]. Vesicles for biomimicking applications are most commonly produced by hydration or electroformation methods. In the hydration method, a thin lipid film is dried on a solid surface and carefully hydrated with an aqueous solution, leading to film swelling and formation of thin-walled vesicles (Figure 2.3). If the sample is significantly agitated during hydration, then MLVs will form instead. The important requirement for formation is that the hydration is performed at temperatures above the liquid-crystalline/liquid-disordered phase transition temperature. This method is suited for vesicle production within a wide range of salt concentrations (up to 2M) and from a variety of lipid mixtures composed of phosphatidylcholine or phosphatidylethanolamine and 10 to 20% of charged lipids [50]. The electroformation or electroswelling technique uses an external electric field during lipid hydration and forms a rather homogeneous vesicle population with a high yield of GUVs. At the same time, the electroformation method has limitations for high concentration of charged lipids in the lipid film and works best at low ionic strength solutions. Vesicle production at physiological and high ionic strength conditions requires special modifications [51-52]. There are several newly developed methods capable of high-throughput production of GUVs [53], overcoming lipid composition and solution ionic strength limitations [54].

In this thesis (Papers I-IV) a modified dehydration-rehydration procedure [55-56] was used, resulting in a population of MLVs (~5-10µm in diameter) with attached thin-walled vesicles (~10-15µm in diameter) referred to as GUVs. MLV-GUV complexes are formed in buffers with physiological ionic strength. The material used for this lipid mixture is mostly SPE with or without minor additional components (Papers III-IV). The method of IR-laser-heating-induced GUV generation from the surface of MLVs [57] greatly expands the range of applicable lipid materials and allows the use of both charged and neutral lipid mixtures.
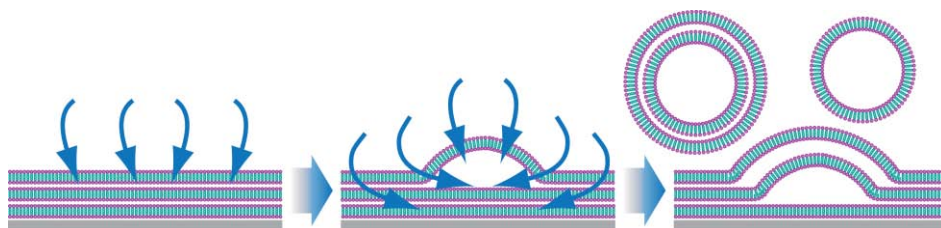
Figure 2.3 Formation of thin walled (uni- and oligolamellar) vesicles from lipid film on a solid support. Solid blue arrows represent hydration process.

2.4. Control of vesicle lamellarity

The unilamellarity of vesicles is particularly important for applications like drug delivery [58] or reconstitution of membrane proteins [47]. One of the ways to evaluate the lamellarity of a fairly homogeneous population of LUVs or GUVs is a fluorescence quenching assay [47, 59]. A small concentration of fluorescently labeled lipids is added to the original lipid mixture. After the formation procedure is complete the vesicles are placed into a spectrofluorimeter cuvette and the drop in fluorescence intensity is monitored, firstly, after the addition of a water-soluble quencher and, secondly, after the addition of a membrane solubilizing surfactant. The ratio of the two intensity drops indicates an average degree of lamellarity in the vesicle population. The lamellarity of individual GUVs can be measured through their elasticity modulus by a micropipette aspiration technique [60].

The lamellarity of GUVs attached to MLVs created by dehydration-rehydration and by the IR laser heating procedure were studied simply by fluorescence imaging with identical excitation intensities and image acquisition settings during all experiments and by comparison of the GUVs intensities [57, 61]. Studies showed that both techniques result in similar lamellarity distributions. The method for determination of the radii of nanotubes pulled from GUV membranes of MLV-GUV complexes (Papers III-IV) provides an alternative way to measure lamellarities. This scheme has been applied to vesicles produced from different lipid mixtures by dehydration-rehydration, and showed that the distribution of lamellarities changed from one material to another.

2.5. Variety of vesicle shapes

Lipid membranes are highly flexible and fluid, while at the same time robust. They convey the properties necessary for cells to deform and squeeze, while moving in the body, without losing their integrity as, for example, erythrocytes passing through capillaries. Erythrocytes are also well known to have non-spherical biconcave disc shape, which changes due to osmotic effects or in the course of certain disease [62].

The observations of the freely suspended vesicles by optical microscopy have shown that they also can exhibit different shapes and shape transitions [63]. These shapes can be mathematically predicted by minimizing the energy for the given vesicle inner volume to surface area ratio and then arranged into phase diagrams describing possible shape transformation [64]. The most commonly observed vesicle shapes are illustrated in Figure 2.4, also representing key steps in these transformations. A spherical vesicle (Figure 2.4A) can transform into a discocyte (Figure 2.4B) and then a stomatocyte (Figure 2.4C) or
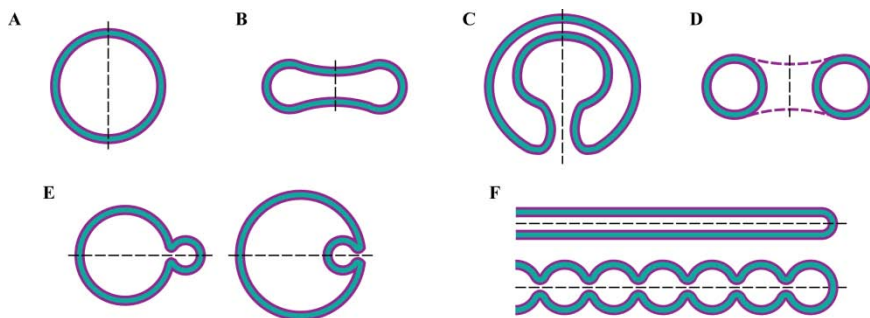
Figure 2.4 Typical morphologies of vesicles suspended in solution. The axis of rotational symmetry is shown with dashed line.

undergo a budding transition (Figure 2.4E). At certain conditions tubular protrusions or chains of pearls can be formed (Figure 2.4F). Occasionally unusual vesicles with non-spherical topology (containing one or more holes) are observed, for example, a torus vesicle (Figure 2.4D) in a shape of a donut. The energy models of the lipid membranes and factors governing vesicle shape transitions will be considered in the Chapter 3.

2.6. Cell plasma membrane blebs

Blebs are spherical protrusions which appear and disappear on the cell surface. They are commonly observed during cell migration [65], mitosis [66] and apoptosis [67]. Typically, bleb growth starts with the detachment of a small section of plasma membrane from the cytoskeleton. If the detachment area reaches a critical dimension, the membrane continues to inflate, forming a spherical bleb of several micrometers in diameter, within approximately 30s [68]. The majority of blebs shrink back within a few minutes with the help of reassembly and contraction of the cytoskeleton cortex and myosin motors.

Irreversible blebbing can be induced by various chemical agents, for example, a mixture of formaldehyde and dithiothreitol (DTT), used in Papers III-IV. In this case, blebs become very large (Figure 2.5) and at some point can bud off from the cell surface; such blebbing represents a technique commonly used to isolate the plasma membrane from cells [69]. Plasma membrane blebs excreted with formaldehyde-DTT protocol have been demonstrated to retain the general characteristics of plasma membranes including exclusive enrichment of certain plasma membrane enzyme markers, high cholesterol-to-phospholipids-ratio and high sphingomyelin content [70]. This is important when considering results presented in Papers III-IV, where the blebbing procedure was applied to study plasma membrane stiffness.
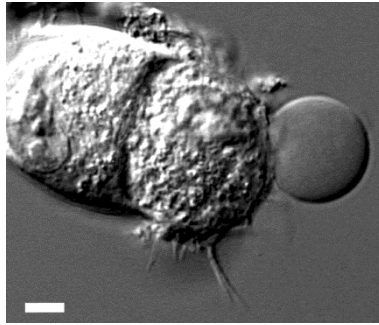
Figure 2.5 DIC image of the NG108-15 cells with attached cell plasma membrane bleb, formed after 30min exposure of the cells to a mixture of formaldehyde and DDT. Scale bar represents 5µm.

2.7. Single cell studies

Cells within a morphologically indistinguishable cell population derived from the same origin (for example, individual neurons in the nervous system, diabetic and normal pancreas beta cells, and cells undergoing embryogenesis and differentiation) are heterogeneous and display differences in morphology, levels of protein expression, behavior and function [71]. When methods of bulk analysis are applied to heterogeneous populations, the obtained information about cell properties can be misleading, often averaging away system-specific information. Understanding the importance of single cell studies has lead to the development of novel tools and techniques [71-72].

One of the technologies which is rapidly expanding and has a great potential for single cell applications is microfluidics. It deals with very small quantities of samples, typically nano- to picolitres, by directing them using devices with micrometer-sized channels [73]. Microfluidics provides new opportunities, for example, the trapping and sorting of live cells, high throughput analysis and single cell stimulation [74].

Many of the methods utilized for biological membrane studies, like electrophysiology [75], manipulations with optical tweezers [76] and fluorescence imaging [77], are in fact dealing with signals from single cells. These techniques used in conjunction with microfluidics provide unique data about membrane protein structures [78] and enable selective probing of the spatially distinct parts of the plasma membrane [79], measurements of the dose-response curves from adhered cells, and extraction of plasma membrane vesicles from single cells (Paper V).

3 MECHANICAL AND CHEMICAL PROPERTIES OF LIPID BILAYER MEMBRANES

Shape transformation processes are coupled to bilayer deformation and deflections from equilibrium state, reflected in the membrane energy. The resistance of membranes to deformation forces originates from the internal organization of lipid bilayers. Therefore, bilayer in a fluid state, above the phase transition temperature, does not resist in plane shear stress, since it is a two-dimensional liquid. Also friction between bilayer leaflets is negligibly small [43]. On the contrary, a much bigger force is required for deformations like stretching, which forces lipid heads to increase their unit spacing and exposes the hydrophobic interior of the bilayer to water. This corroborates why membrane mechanical characteristics are sensitive to factors which affect lipid packing, such as the addition of membrane components or the effects of the surrounding solution.

This chapter summarizes the theoretical background behind membrane deformation, adhesion and electroporation, necessary to understand the transitions of vesicle shapes and the procedure for the formation of NVNs.

3.1. Membrane stretching

One of the best ways to understand lipid membrane behavior under the influence of a stretching force (Figure 3.1A) is to utilize micropipette aspiration of GUVs [80]. The scheme of the experiment is shown in Figure 3.1C. The tension σ (force per unit length), applied to the GUV membrane of original area A_0, is regulated by the difference between pressure in the micropipette with radius R_p and in the surrounding solution (Δp). The applied tension is redistributed over the entire GUV surface and results in a different vesicle radius (R_v), length of protrusion (L) and, consequently, a new surface area (A) for each value of Δp. At first, when the applied force is small, the vesicle area grows exponentially with increasing tension, but after some threshold ($\sigma \sim 10^{-4}$N/m) the dependence becomes linear. These two regimes can be explained by thermal undulations in the unstressed membrane, which gradually straightens out due to the growing tension until the bilayer is flat (Figure 3.1D), giving an exponential expansion of the membrane area. In the linear regime, area dilation ($\Delta A/A_0 = (A - A_0)/A_0$) is governed by actual bilayer stretching and, based on the Hooke's law, results in an increase of the free energy per unit area (f_{str})

$$f_{str} = \frac{K_A}{2}\left(\frac{\Delta A}{A_0}\right)^2 = \frac{\sigma}{2} \cdot \frac{\Delta A}{A_0} \qquad (3.1)$$
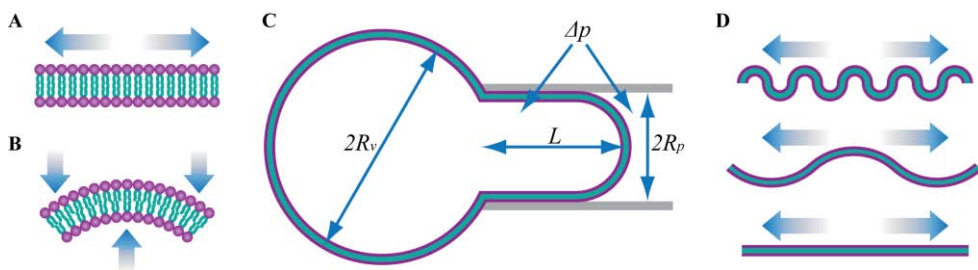
Figure 3.1 Modes of the lipid membrane deformation. Parameters of the membrane resistance to two main modes of deformation, stretching (A) and bending (B), are often measured by micropipette aspiration of GUVs (C). At first membrane stretches exponentially, which corresponds to restriction of the thermal shape fluctuations (D), and then linearly, until the vesicle raptures. Gradient arrows show direction of the applied force.

The coefficient K_A, is the membrane stretching or area compressibility modulus. Its value is usually in the range of 0.08-0.2N/m for lipid membranes [80-83].

In fact, membrane stretching is an extremely unfavorable process which only makes possible an area expansion up to a maximum of 3-5% at tensions of around 5-10mN/m [43, 84]. With increasing tension the membrane ruptures and the vesicle is destroyed. Therefore, in many cases, including papers presented in this thesis, an assumption of a constant surface area is valid.

3.2. Membrane bending

The thickness of the lipid bilayer is only 5nm, which facilitates bending. Resistance of the membrane to bending deformation (Figure 3.2B) is characterized by the bending modulus or bending rigidity κ, typically measured to be in the order of 10^{-19}J [43]. The bending rigidity is one of the most important parameters for vesicle shape transformations since it describes the creation of membrane curvature.

There are two classic methods to measure bending rigidity of bilayers in natural environments. The oldest method is flickering spectroscopy [85], where κ is extracted from the shape of directly observed thermo-induced fluctuations. The other method is micropipette aspiration [80], the same as was described for membrane stretching above (Figure 3.1C). The bending rigidity is so low, that it is very difficult to determine the exact numerical value, and the values measured with different techniques often diverge by a factor
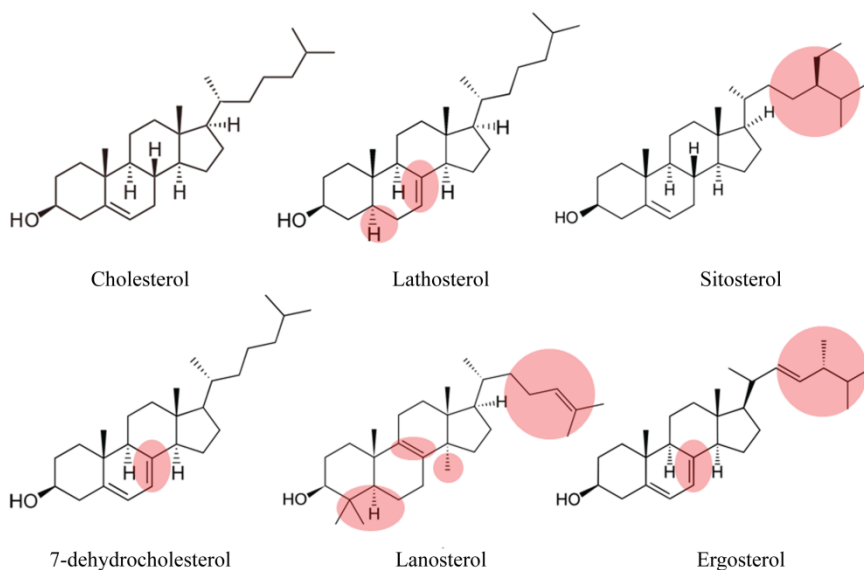
Figure 3.2 Examples of sterols' chemical structures. The variations from cholesterol structure are pointed with red color.

of 1.5-2 [86]. Even within one technique applied to the same material the values can alter significantly, depending on exact experimental conditions, for example, the sugar concentration in the solution. This shows that the bilayer cannot be considered only by itself, because its properties are very sensitive to the environment. Interactions even with such small molecules as inorganic ions can sufficiently alter membrane mechanical properties, bilayer thickness and rates of lateral diffusion in the membrane [87].

The bending rigidity of the membrane originates from ordering of the lipid molecules in the bilayer and evidently depends on the lipid composition used. One of the classic examples is cholesterol which makes membranes both stiffer and more difficult to stretch [80] by enhancing the packing of fatty-acid chains. Cholesterol is the main sterol of animal cells. It adjusts membrane permeability and fluidity to the physiologically required levels, promotes lateral organization of the membrane, such as raft formation [1], and participates in essential processes, like intracellular vesicular trafficking [88] and endocytosis [89]. The common approach to study cholesterol functions in the cell is plasma membrane cholesterol extrusion with methyl-beta-cyclodextrin (MβCD) [89], also used in Paper IV.

Cholesterol belongs to a group of lipids called sterols, naturally occurring in animals (cholesterol), fungi (ergosterol) and plants (sitosterol). In spite of their similar chemical structure (Figure 3.2), sterols effect on membrane properties, including bending rigidity [90]

(Paper IV), can be very different and has serious consequences for a living organism. For example, abnormalities in cholesterol synthesis and accumulation of its precursors (7-dehidrosterol and lathosterol) result in deviations in normal cellular processes and diseases [27].

3.3. Membrane curvature and the Spontaneous-Curvature model

The easiest way to look at the curved lipid membrane is to neglect its thickness and simply consider it as a surface. The bent surfaces can be described in terms of the principle curvatures. Curvature of the smooth curve in a two-dimensional space at a given point is the reciprocal of the osculating circle radius. At each point of the surface in three-dimensional space, two perpendicular principal directions in which the surface bends the most and the least can be defined. Intersections of the normal planes in these directions with the surface will correspond to the maximum and minimum values of curvature at the given point, which are called principle curvatures. Figure 3.3 illustrates principal directions and corresponding principle curvatures (C_1 and C_2) for three basic lipid membrane conformations: planar bilayer, spherical vesicle, and tubular.

The Spontaneous-Curvature model of the membrane [91] defines the curvature or bending energy (F_{curv}) of the vesicle as a sum of integrals over all vesicle area (A)

$$F_{curv} = \frac{\kappa}{2} \oint (C_1 + C_2 - C_0)^2 dA + \kappa_G \oint C_1 C_2 dA \qquad (3.2)$$

The first term gives contribution of the bending deformation and spontaneous curvature (C_0) into energy. C_0 describes possible asymmetry of the lipid bilayer, and is equal to zero, when membrane leaflets are identical [63], as in the MLV-GUV vesicle complexes used in this thesis. The second term contains the Gaussian bending modulus (κ_G) and describes membrane topology. It is used to model membrane fusion, but in the context of this work, can be omitted, since the topology remained the same in all presented experiments [92]. So the simplified expression for curvature energy of symmetrical bilayers of fixed topology is

$$F_{curv} = \frac{\kappa}{2} \oint (C_1 + C_2)^2 dA \qquad (3.3)$$

Now it is easy to see that curvature energy of a spherical vesicle of radius R is
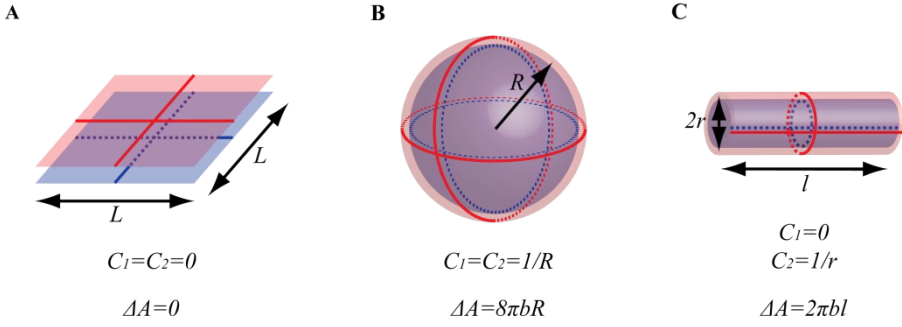
Figure 3.3 Principal curvatures (C_1 and C_2) and difference in leaflets surface area (ΔA) for elemental membrane geometries; plane (A), sphere (B) and cylinder (C). Neutral surfaces of outer (red) and inner (blue) membrane leaflets separated by a distance equal to half of bilayer thickness (b) and principal directions on the surface (red and blue lines) are shown.

$$F_{curv}^{sphere} = \frac{\kappa}{2} \oint \left(\frac{1}{R} + \frac{1}{R} \right)^2 dA = 8\pi\kappa \qquad (3.4)$$

and does not depend on the vesicle radius, while the bending energy of the membrane folded into a tube with radius r and length l is

$$F_{curv}^{tube} = \frac{\kappa}{2} \oint \left(0 + \frac{1}{r} \right)^2 dA = \frac{\kappa\pi l}{r} \qquad (3.5)$$

and grows with decreasing tube radius. For example, the surface area of a membrane tube with $r = 50$nm and $l = 40$µm is equal to surface area of a vesicle with $R = 1$µm, but the curvature energy of the tube is $800\pi\kappa$, a hundred times larger than energy of the spherical vesicle. The sphere is the lowest energy state of all vesicles of simple topology.

3.4. Area-Difference Elasticity model and interleaflet lipid transport

In reality, lipid bilayers have a finite thickness (~5nm) and neutral surfaces of inner and outer leaflets are separated by a certain distance (b). As shown in Figure 3.3, for a plane, a sphere and a tube, this means that membrane geometries require different surface areas for two leaflet surfaces. The Area-Difference Elasticity model of a lipid membrane [93] considers a situation when the membrane at equilibrium (or relaxed) with leaflet areas (A_0^{in} and A_0^{out}) is subjected to bending deformation, and migration of lipids between the bilayer

leaflets is forbidden. Under these conditions, the number of lipid molecules in the leaflets cannot adjust to the new shape. As a result, relative stretching of the leaflets to new actual areas (A^{in} and A^{out}), which can be higher or lower then A_0^{in} and A_0^{out}, occurs. The Area-Difference Elasticity model describes this with an additional term in the expression for the membrane elastic energy (F_{ADE})

$$F_{ADE} = \frac{\kappa}{2} \oint (C_1 + C_2 - C_0)^2 dA + \frac{\pi\bar{\kappa}}{2Ab^2}(\Delta A - \Delta A_0)^2 \qquad (3.6)$$

$$\Delta A = A^{out} - A^{in} = b \oint (C_1 + C_2) dA \qquad (3.7)$$

$$\Delta A_0 = A_0{}^{out} - A_0{}^{in} \qquad (3.8)$$

where $\bar{\kappa}$ is en effective non-local bending modulus.

The area difference does not relax due to lipid molecule transport between the leaflets (flip-flop), because the rate of this process is extremely slow (to the order of hours) [94]. Although the preferred area difference can be changed over time by some conditions, such as the acceleration of the flip-flop rate by special enzymes [95] or lowering the lipid molecule concentration in the outside solution below CMC [18]. There are also reports of accelerated rates of interleaflet lipid translocation (~10min) in highly curved membranes [20] (Paper I), but it is problematic to determine the exact translocation mechanisms, and it is likely that accelerated interleaflet transport occurs through small defects in the membrane bilayer [96].

3.5. Membrane permeability

The permeability through the lipid bilayer depends on the ability of certain species to pass through the hydrophobic core of the membrane. The membrane is generally permeable to small nonpolar molecules, like CO_2 or O_2, since they can dissolve in the bilayer. Small uncharged polar molecules, such as water, diffuse through the membrane at a slower rate. The membrane permeability coefficient for water is in the order of 10^{-2}-10^{-3}cm/s [97]. In contrast, the membrane is almost impermeable for charged molecules, even for small ones, like ions. Ion permeability coefficients are around 10^9 times lower than for water. For example, the permeability coefficient for potassium ions is around 10^{-10}-10^{-12}cm/s [97]. The major difference between ion and water permeability coefficients makes the lipid bilayer act as a semipermeable membrane. The transport of water solution with ion concentration c_S

through the membrane is described by the Kedem-Katchalsky equations [98] in terms of solute (ions) flow (J_S) and volume flow (J_V), consisting of combined water and solute flow,

$$J_V = L_p(\Delta P - \sigma \Delta \Pi)$$
(3.9)

$$J_S = \omega \Delta \Pi + c_S(1 - \sigma)J_V$$
(3.10)

where L_p is a filtration coefficient, ω the solute permeability, σ is the reflection coefficient, which characterizes membrane selectivity against solute, ΔP and $\Delta \Pi = RT\Delta c_S$ are the hydrostatic and the osmotic pressure jumps over the membrane, R is the universal gas constant and T the absolute temperature. Externally induced osmotic pressure can lead to swelling or shrinking of the vesicle volume by the selective transport of water to equilibrate solute concentrations and to changes in the vesicle shape [99-101]. On the other side, if there is no concentration difference, it is problematic for the inner volume of the vesicle to change, since it will lead to osmotic imbalance, as is discussed in Paper I.

3.6. Shape transformations under external stimuli

A variety of equilibrium vesicle shapes is explained by minimization of the membrane energy for a fixed encapsulated volume and surface area. Changes in parameters related to vesicle energy, surface area or volume lead to changes of vesicle shape. Most of the times methods for vesicle preparation result in spherical vesicles. That is why studies of shape transformation mechanisms mainly consider spherical vesicles as a starting point. Sphere-discocyte-stomatocyte transitions and formation of buds are the most common shape transitions.

The earliest studies describe shape transitions due to a change in either the temperature or the osmotic gradient through the membrane. The thermo-induced shape fluctuations were explained by a small difference in the thermal expansion of two leaflets produced by residual impurities [102]. In case of a change in the osmotic pressure, the vesicle volume is forced to adjust until water equilibrates the ion concentrations inside and outside the vesicle. This often results in formation of tubular protrusions or chains of pearls connected by a narrow neck [17, 100]. The other way to induce shape transformations is a direct application of force (for example, with optical tweezers [16]), which increases the membrane tension. The vesicle shape is also sensitive to changes in the difference between the equilibrium areas of membrane leaflets, described in the Area Difference Elasticity model. Experimentally, such changes can be achieved, for example, by lowering the lipid monomer concentration in the outside solution below CMC [18] or by transport of the lipids between the leaflets mediated by special enzymes [95].

17

Several studies report shape transformations of thick tubular membrane structures. They exhibit pearling instability when affected by applied surface tension [16], increase in spontaneous curvature due to intercalations of polymer chains [103] or nanoparticle-induced changes in effective head group area and membrane bending rigidity [104]. For the nanoscale structures, like nanotubes, even when the shape transformation can be observed by optical microscopy [19, 105], it is difficult to follow the variations of the membrane geometry and to determine the exact transformation mechanisms.

3.7. Electroporation and electrofission

Electroporation of cell plasma membranes has found a variety of applications ranging from transfections and preparation of hybridoma cells [106-107] to the selective destruction of targeted cells in tissue for medical purposes [108]. Electroporation can also be used for manipulating the vesicle membrane, performing electrofusion [22, 109], electrofission [19] (Paper I) and electroinjection [11] (Papers I-IV).

Lipid membranes in an electric field can be thought of as capacitors, where two lipid head planes play the role of the conducted plates and the hydrophobic interior of the membrane acts as an insulating (dielectric) layer. When an electric field is applied across the membrane, the charge densities on both sides of the membrane are changed. A low dielectric constant of bilayers ($\varepsilon_m \sim 3$ [110]) ensures that the charge is stored on the bilayer sides. The typical capacitance of model lipid bilayers is $\sim 2\mu F/cm^2$.

At high electric field strength, dielectric breakdown starts to occur, the bilayer become destabilized, and hydrophobic defects appear (Figure 3.4A-B) and develop into nanosized hydrophilic pores (Figure 3.4B-C) [111] with an energy defined by the pore radius (a) and the line tension (γ) [112]

$$E_{pore} = 2\pi a \gamma - \pi a^2 \sigma$$

(3.11)

The fate of the pore is defined by the balance between the energy necessary to form the edge of the pore (first term) and energy gain when pore size is growing under surface tension σ (second term). If the electric pulse was long and high enough, then electroporation will occur irreversibly, and the size of the formed pores will exceed a critical dimension and grow under action of the surface tension until the membrane ruptures. Irreversible electroporation was used in Paper I to release membrane nanotubes from NVNs. If the pore size does not reach critical dimensions, electroporation will be reversible and the pores will close. The typical life of such pores is in the order of microseconds. The formed pores have
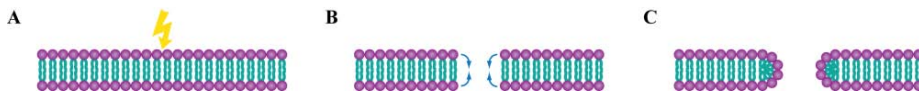
Figure 3.4 Electroporation of a lipid bilayer. Application of a short electric pulse to the intact bilayer (A) leads to localized rearrangement of the lipids, initiation of hydrophobic defects (B) and formation of the pore (C).

an aqueous interior. This temporarily allows the transport of water soluble compounds through the bilayer and also assists the penetration of the membrane with a glass micropipette (Papers I-IV).

3.8. Vesicle adhesion

Vesicles suspended in solution will settle on the surface. The head groups of the outer vesicle leaflet in close proximity to the surface experience Van der Waals, electrostatic and hydration effects, which define the degree of membrane surface interaction. To describe the adhesion in a convenient way, an effective contact potential (ϕ) is introduced. The energy of the vesicle then has an additional term [113]

$$E_{adh} = -\phi A^*$$

(3.12)

where A^* is the contact area between the surface and the vesicle. For isolated GUVs, without a connection to the lipid material reservoir, surface adhesion is balanced by the stretching energy, and the size of the contact area depends on value of the contact potential (Figure 3.5).

The adhesion characteristics of the surface are extremely important for producing NVNs by the micromanipulation technique. If the contact potential is low, the vesicle will
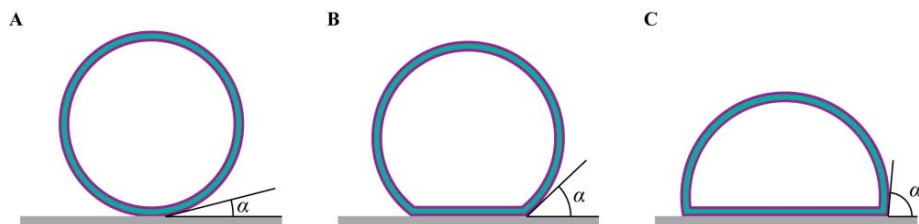
Figure 3.5 Surface adhesion of vesicles with different effective contact potentials.

19

not adhere to the surface (Figure 3.5A) or the adhesion will be insufficient for the vesicle to be held in place during micromanipulations. If the contact potential is too high, the vesicle becomes too flat (Figure 3.5C) to work with and can also easily rupture and spread on the surface, forming a supported lipid bilayer. In Papers I-IV specially prepared surfaces were used for NVN production to ensure a proper level of vesicle adhesion (Figure 3.5B) and stability of the created networks.

4   LIPID MEMBRANE NANOTUBES

Lipid membrane nanotubes or tethers are cylindrical entities with radial dimensions ranging from tens to hundreds of nanometers. Their size makes them a useful model for cellular membrane structures. Originally, membrane tethering was observed in red blood cells subjected to fluid shear stress [114]. Presently there are several methods to extract nanotubes from both artificial as well as cell membranes. They are used, among many other things, to model the action of membrane remodeling proteins [49, 115] and to study the elastic properties of plasma membranes and the underlying cytoskeleton [116-117].

In this thesis (Papers I-IV), nanotubes were formed as part of NVNs. The main advantage of this technique is the ability to build structures with desired geometry and connectivity, while controlling the internal aqueous environments of each vesicle in the network. It enables the investigation of membrane shape optimization and transport within the nanotubes. This chapter will discuss the NVNs construction procedure, the theory behind nanotube mechanics and modes of the transport within the networks. Several effects connected to the induction and relaxation of the membrane surface tension gradients, important for the presented work, are also considered.

4.1. Nanotube pulling

Nanotubes are generated when a highly localized force is applied to a lipid membrane. In nature, this is achieved through the action of motor proteins or polymerization of the cytoskeleton filaments [118]. Experimental setups commonly use optical [119] or magnetic [120] tweezers, or a glass micropipette attached to a micromanipulator [56]. Both experimental and theoretical data show that a significant energy barrier should be overcome to initiate formation of the nanotube from a flat membrane [118] with an initial force around 10% higher, than the force required to continue tube elongation (~10pN) [121]. A membrane arranged into a nanotube conformation has high curvature energy and the nanotube is an equilibrium shape only while the force remains. The free energy of a nanotube with radius r and length l is

$$F_{nanotube} = 2\pi r l \sigma + \frac{\pi \kappa l}{r} \tag{4.1}$$

The ends of the pulled nanotube should be fixed; otherwise the tube will retract back to the originating membrane. In cases where both ends are released close in time, the nanotube undergoes shape transformation to lower the energy [105].

The radius of the nanotube is determined by the balance of tension (σ) at the membrane surface and the ability of the membrane to resist bending described by the bending rigidity (κ) [122] and can be found from

$$\frac{\partial f_{nanotube}}{\partial r} = 0 \qquad\qquad (4.2)$$

where $f_{nanotube}$ is the nanotube energy per unit length

$$f_{nanotube} = 2\pi r\sigma + \frac{\pi\kappa}{r} \qquad\qquad (4.3)$$

which leads to the expression for the radius

$$r = \sqrt{\frac{\kappa}{2\sigma}} \qquad\qquad (4.4)$$

4.2. Nanotube vesicle networks

The protocol for the preparation of NVNs is described in detail in Paper II and pictorially summarized in Figure 4.1. NVNs can be readily prepared from surface adhered MLV-GUV complexes [11] (Figure 4.1A-E) or cell connected plasma membrane blebs [33] (Figure 4.1G). The MLV or cell serves as the membrane material reservoir, while the membrane of the GUV or bleb is subjected to series of micromanipulations.

The MLV-GUV complexes or plasma membrane blebs are contained in a buffer bath situated on a conventional inverted microscope. They are approached with a sharp glass pipette (Figure 4.1A) with a submicrometer opening. This micropipette is prefilled with the solution of choice, connected to an injection pump and fitted with an electrode for electroporation. A second electrode is placed in the buffer bath. The micropipette tip is forced against the GUV or bleb membrane with the simultaneous application of mechanical force and an electric field, piercing the membrane (Figure 4.1A-B). The tip is withdrawn from the GUV or bleb, forming a nanotube due to the attachment of the membrane to the glass micropipette. Application of a slight positive pressure to the pipette inflates the tube, forming a new daughter vesicle (DV) (Figure 4.1B-C). This injection pressure can be adjusted to control the size of the DV (Figure 4.1C-D). The DV can then be placed on the surface by micromanipulation (Figure 4.1D-E) stabilizing the nanotube by vesicle adhesion, which prevents tube shortening and vesicle fusion. The DV can be adhered to any place on the surface defining the nanotube length and network geometry. After attachment of the DV
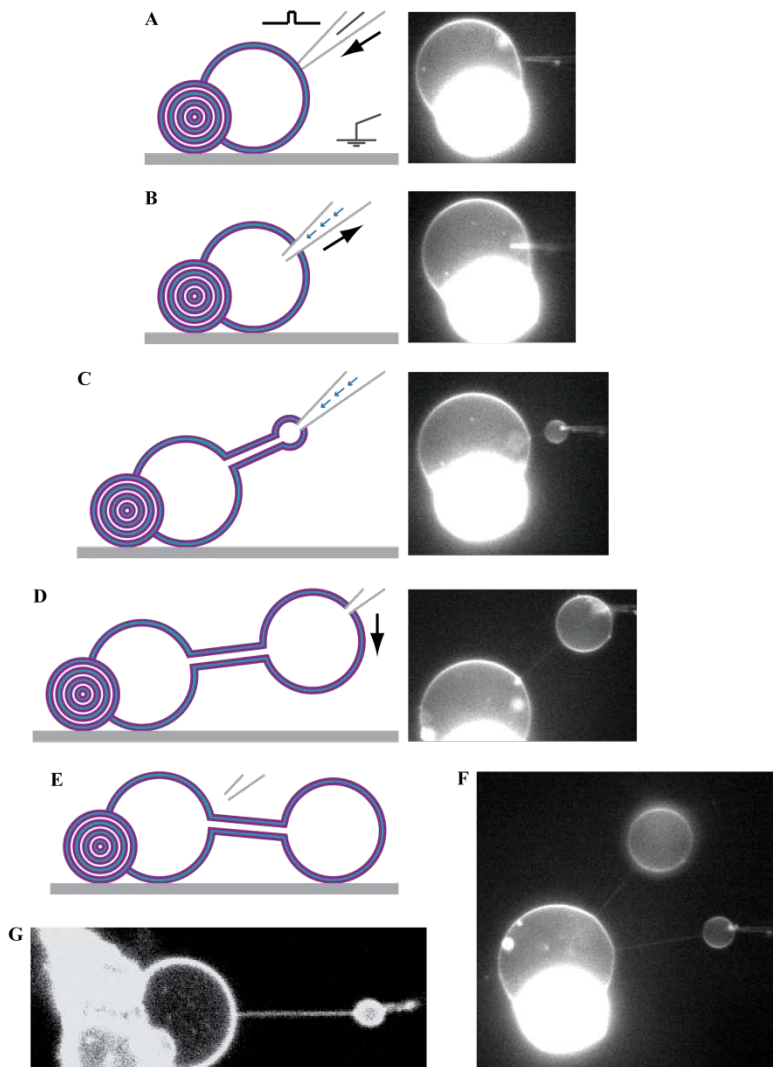
Figure 4.1 Schematic illustrations and fluorescence microscopy images of formation of the NVNs. (A-B) Glass micropipette is pushed into GUV's membrane with simultaneous application of several electric pulses, until pipette tip penetrates the membrane. (B-C) Injection pressure is increased and pipette tip is withdrawn from GUV, leading to formation of nanotube and DV. (C-D) Injection of the solution through the pipette can be continued until DV reaches desired size. (D-E) The DV can then be positioned on the surface and separated from the pipette, with is now ready for the formation of the next DV and more complex network (F). In the same manner NVNs can be built from the membrane of the cell connected plasma membrane blebs, (G).

to the surface, the micropipette can be withdrawn from the DV, and subsequently used to repeat the steps and build complexity into the network as in Figure 4.1F. This micropipette can also be used to perform electrofission and release the nanotube to freely float in the solution as in Paper I.

4.3. Shape optimization

A high degree of control over the geometry of NVNs provides an opportunity to build structures whereby the membrane is kinetically trapped in a stable high energy state. A predetermined trigger could then be implemented to induce a change in the system, enabling the observation of the energy minimization process. This approach has been utilized to study optimization of the membrane shape.

One of the simplest examples is a V to a Y shape transition [13], illustrated in Figure 4.2A. At the beginning of the experiment a V-shaped three vesicle network is built. The
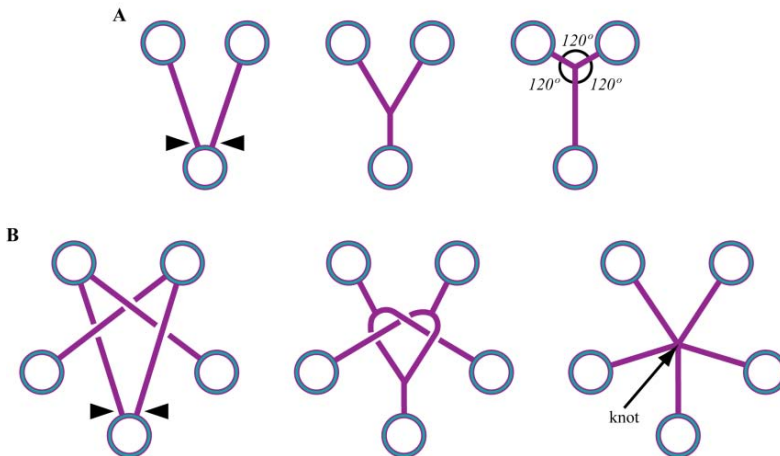
Figure 4.2 Dynamic shape optimization in NVNs. (A) Once two nanotubes are forced to fuse (black arrows), the V-shaped network transforms into the Y-shape with minimal total nanotube length, corresponding to the equal 120º degree angle between three joined nanotubes. (B) In more complex networks, the final structure depends on original position of the nanotubes in three-dimensional space, and nanotube knots can be formed instead of 120º degree Y-junctions, although knot formation also minimizes nanotube length for given network configuration.

network is stable; because the ends of two nanotubes are spatially separated and cannot fuse without external influence, but they can be brought together by applying a mechanical force and an electric pulse (Figure 4.2A, black arrows). Once fused, the nanotubes reorganize into a Y shape. As it is discussed in section 4.1 the nanotubes are the highest energy component in the system, and their energy is proportional to the total tube length (eqn. 4.1), so the fusion continues until conformation with the minimal nanotube length and energy (Y-junction with 120º degrees angle between nanotubes) is reached. This transition typically takes several seconds to complete.

In the case of more complex networks, the result of shape optimization can vary depending on the network geometry and three-dimensional positions of the nanotubes relative to each other. The final structure can consist of a combination of several Y-junctions with 120º degrees angles between the nanotubes [12] or various knots can be formed [14]. An example of a knot is shown in Figure 4.2B. Nevertheless, in both scenarios the nanotube length is minimized during shape optimization.

Using a combination of the NVN technique and electrofission it is possible to release prepared tubular structures, for example a torus [19], to float freely in the solution and observe their dynamic shape transformations. In Paper I this approach is applied to produce and study the transformation dynamics of long linear nanotubes.

4.4. Nanotube radius

The typical range of nanotube radii is from tens to hundreds of nanometers, well below the diffraction limit of optical microscopy. This makes it challenging to measure the radii directly, under natural conditions, and explains the need for quantitative techniques. Figure 4.3 illustrates two methods which were both used to measure the radii of SPE lipid membrane nanotubes in similar systems, but lead to significantly different values.

The first technique [25] (Figure 4.3A) uses the concentration gradient (ΔC) of electroactive molecules (catechol) with a diffusion constant D, extracting the inner nanotube radius (r_{in}) from the recorded change in current (Δi) and Fick's first law of diffusion

$$r_{in} = \sqrt{\frac{\Delta i}{nF\pi D \frac{\Delta C}{L}}} \qquad (4.5)$$

where L is a nanotube length, F is Faraday's constant and n is number of electron transferred per electroactive molecule. The obtained radii depended upon whether the nanotube was

connected directly to the pipette or to a small vesicle. The average value was 57nm and 24nm, respectively.

In the second technique [24, 119] (Figure 4.3B), two nanotubes of length L_t are pulled from the same vesicle with radius R_v, and the angle between them is decreased until they fuse and form a Y-junction. The merging angle (θ) corresponds to nanotube outer radius value (r_{out})

$$r_{out} = \frac{\theta^2 R_v \left(1 + \frac{R_v}{L_t}\right)}{4} \qquad (4.6)$$

measured to be around 110nm for SPE nanotubes.

Paper III in this thesis proposes an alternative approach to nanotube radius measurement. It has the fidelity to identify the inhomogeneity in vesicle population lamellarity and explains variation in previously obtained values.

In general, the nanotube radius is determined by a balance of stretching and bending forces at the membrane surface and is described by eqn. 4.4. The bending rigidity κ, represents membrane properties and can be influenced by membrane composition and the local environment, while membrane tension σ represents the external force applied to pull the nanotube. When nanotubes are extracted from separated GUVs held by an aspiration pipette, then the membrane tension is an important factor which can significantly change the radius value. In this work all nanotubes were connected to a lipid reservoir, which unrolls
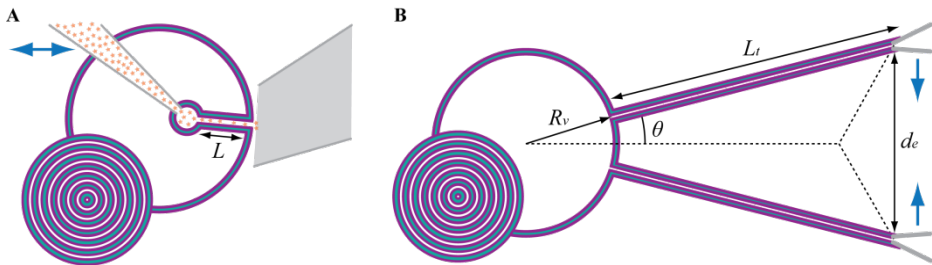
Figure 4.3 Methods of nanotube radius measurement in natural conditions. (A) Inner nanotube radius is determined from a current induced by a flux of electroactive molecules through the nanotube. (B) The outer nanotube radius is determined from the angle at which two nanotubes pulled from the same vesicle merge to form a Y-junction.

when the tubes are created and extended, ensuring that no additional tension is induced in the network. The tension can be assumed to be constant and equal to the equilibrium value (~10^{-6}N/m for MLV-GUV complexes [13]). In a system where the membrane tension is buffered by the presence of the lipid reservoir, the nanotube radius directly reflects the bending properties of the bilayer. This was used in Paper IV to monitor changes in membrane bending rigidity.

4.5. Diffusion through a nanotube

When the NVNs are built, it is possible to inject different materials into each vesicle by changing the solution in the micropipette. Networks prepared in this way are useful to study transport of soluble and membrane-bound materials.

The most evident way that a solute concentration difference can equilibrate between vesicles is through diffusion. Equilibration of the concentration gradients by diffusion is a consequence of Brownian motion. In NVNs it is a valid transport mode for particles that are smaller than the diameter of the nanotube, for example, small fluorophores or enzymes [23].

Diffusion is characterized by the diffusion constant (D), the coefficient of proportionality between the molar flux and the concentration gradient. The diffusion constant of spherical particles with radius a in systems with low Reynolds numbers, such as NVNs, is described by the Stokes-Einstein equation

$$D = \frac{k_B T}{6\pi \eta a}$$

(4.7)

where k_B is Boltzmann's constant, T is the absolute temperature and η is viscosity of the solution. The characteristic time for mixing by diffusion (t_{mix}) in a container with a characteristic length scale L is given by,

$$t_{mix} = \frac{L^2}{D}$$

(4.8)

For example, the mixing time for particles with a diffusion constant of 10^{-11}m^2/s in a 10µm diameter vesicle would be 10s. The relaxation time (t_{rel}) for equilibration of the concentration gradient between two chambers with volumes V_1 and V_2 joined by a cylindrical capillary [123] with length L_t and radius R_t (around 50nm for the lipid nanotubes) is calculated to be

$$t_{rel} = \frac{L_t}{\pi D R_t^2} \cdot \frac{V_1 V_2}{V_1 + V_2} \qquad\qquad (4.9)$$

Accordingly, even for two 10µm vesicles connected with quite a short 5µm nanotube, it will take hours ($t_{rel} \sim$ 5h) to equilibrate the concentration levels. The limiting factor of the diffusive transport is the time (t_{ent}) for the particle to find the small nanotube opening from the relatively large volume of the vesicle container,

$$t_{ent} = \frac{R_v^3}{D R_t} \qquad\qquad (4.10)$$

where R_v is the vesicle radius. It takes at least several minutes for the particle to enter the nanotube.

Diffusion is a passive mode of transport, effective only for small particles and short nanotubes. However, there are ways for active transport through nanotubes. In the two following sections two active modes, electrophoresis- and tension-driven transport, are described. They allow the transport of particles larger than the nanotube diameter, like bacteria [124] or large fluorescent beads [24], and can also offer increased transport rates.

4.6. Electromigration through a nanotube

Electrophoresis has been used to transport DNA [125] and latex particles [126] through lipid membrane nanotubes with velocities in the range of ~1-100µm/s. In these experiments, an electric field (~1000V/m) is applied inside the nanotube using two glass-micropipette-based Ag/AgCl electrodes. The proportionality coefficient between the particle migration speed and the applied field strength is referred to as electrophoretic mobility (μ_{ep}) and depends on both the particle size (a) and charge (q)

$$\mu_{ep} = \frac{q}{6\pi\eta a} \qquad\qquad (4.11)$$

Other than the electrophoresis of charged particles of interest, the electric field also drives electroosmotic and membrane flow (Figure 4.4). Electroosmotic flow is related to the electric-field-induced movement of the electrical double layer, existing at the interfaces of solid surfaces and fluid solutions. The membrane flow is caused by electrophoresis of the charged membrane components. Theoretical calculations [126] show that the typical membrane movement is 10% slower than electroosmotic flow, and those two effects balance each other, resulting in a negligible net liquid flow through the nanotube [24].

Figure 4.4 Schematic illustration of a typical setup for electromigration experiments. Electric field is applied with special Ag/AgCl electrodes, based on glass micropipettes filled with gel (blue). Electric field induces electrophoretic movement of charged particles (v_p), electroosmotic flow (v_{eo}) and electrophoretic membrane flow (v_m). Electroosmotic and membrane flows ideally balance each other, so that bulk liquid flow is negligible.

4.7. Marangoni flow and tension-driven transport through a nanotube

The Marangoni effect is the flow along an interface between two fluids to equalize the difference in surface tension, a phenomenon, which can be observed in lipid membrane systems [127]. In NVNs, a tension gradient can be generated by compression or inflation of the DV (Figure 4.5A). In both cases the membrane will start to flow from lower to higher tension regions, inducing Marangoni flow of the solution inside and outside the nanotube (Figure 4.5B). At the same time compression or inflation leads to a pressure difference and Poiseuille flow (Figure 4.5C) in the opposite direction. Marangoni flow dominates in the NVNs [128], therefore the resulting flow (Figure 4.5D) can be used to transport solutes into the vesicle experiencing a higher surface tension.

The time to transport a fraction (*f*) of the vesicle volume (*V*) through the nanotube with length *l* and radius *r* is given by [128]

$$t_{tr} = \left(\frac{R}{r}\right)^3 \frac{\eta l}{\Delta \sigma} \cdot f \qquad\qquad (4.12)$$

where *R* is the vesicle radius and $\Delta\sigma$ is the difference in surface tension. With this method 10^{-12} to 10^{-18} L volume fractions can be transferred in the minute range and the membrane velocities along the nanotube are ~10µm/s [129].

29

Figure 4.5 Marangoni flow. (A) Difference in surface tension between the vesicles in the network, induced, for example, by deforming one of them with micropipette, leads to membrane flow to the regions of higher tension, followed by surrounding solution flow (J_M) **(B)**. This flow competes with Poiseuille flow (J_P) **(C)** induced by pressure difference. In NVNs Marangoni flow is usually higher than Poiseuille flow, therefore the resulting flow (J) profile looks like one shown at **(D)**.

4.8. Relaxation of membrane tension gradients on nanotube membrane

Tension gradients generated on the nanotube surface during various manipulations disturb the membrane in two ways (modes) [128]. The first mode is associated with the actual membrane stretching and fluctuations of the lipid density. The second mode is related to deviations of the nanotube radius from its equilibrium value along the nanotube. These effects are important to consider when performing and analyzing experiments with dynamically changing networks. Theoretical estimates show that the stretching fluctuations' relaxation time is in order of milliseconds, while the relaxation of nanotube radius takes much longer, up to several seconds.

In this thesis careful consideration of the fluctuations produced by tension gradients are particularly important for Papers I, III and IV. In Paper I, unwanted membrane and liquid flows are induced during electrofission of the membrane. Despite that the total experiment time is much longer than several seconds; the respective tension gradients can influence dynamics of the initial stages of the observed shape transformations. In Papers III and IV measurement of the nanotube radius is performed while inflating the DV. To ensure that the radius value is not changed by induced fluctuations special care was taken to minimize the tension gradient and use time periods larger than relaxation times.

During the swelling of the DV by injecting the solution through the micropipette, as illustrated in Figure 4.1C-D, the generated tension can be estimated from a force balance between friction drag forces on the nanotube surface and the tension gradient ($d\sigma/dx$) [128]

$$r \frac{d\sigma}{dx} = \frac{4v\eta}{ln\left(\frac{l}{r}\right) - \frac{1}{2}}$$

<div align="right">(4.13)</div>

where r and l are the nanotube radius and length, and $v = \Delta l/\Delta t$ is the rate of membrane material transfer along the nanotube. This formula has been used in Papers III and IV to ensure that induced tension gradients are lower or in order of the equilibrium tension in MLV-GUV membrane.

If membrane tension increases so rapidly that the nanotube radius cannot equilibrate, instabilities in the nanotube shape, like formation of moving pearl or chain of pearls, are observed. The threshold tension (σ_{pearl}) for this phenomena is given by [16]

$$\sigma_{pearl} = \frac{\kappa}{r^2}$$

<div align="right">(4.14)</div>

Taking typical bending rigidity $\kappa = 4 \cdot 10^{-20}$J and nanotube radius $r = 50$nm gives the threshold tension value $1.6 \cdot 10^{-5}$N/m.

5   IMAGING TECHNIQUES

Due to their small size, vesicles and cells require a microscope to be visualized and manipulated. Optical microscopy uses a system of lenses to produce magnified images of a sample, which can then be directly observed by the human eye or recorded using digital cameras. An image is formed when passing light interacts with the specimen; some objects absorb and/or scatter the light, reducing the local intensity, forming a contrast image. Samples built from lipid membrane are almost completely transparent and require contrast enhancing techniques, such as differential interference contrast (DIC) microscopy. An alternative to this direct method is to employ a tracer, targeting the region or molecule of interest. The tracer probes, typically fluorescent dyes within life sciences, allow for selective monitoring of key labeled component using wide-field or confocal fluorescent microscopy. In this case the membrane labels adsorb illumination light of a specific wavelength, elevating an electron from ground state to an exited state, which then relaxes by emitting photon of a shifted wavelength. Long term imaging with fluorescence microscopy can be problematic due to photobleaching (photochemical destruction) of the dye. Nevertheless, fluorescence microscopy can be used for quantitative measurements (Paper I) and as a tool for tracing membrane movement, using photobleaching (Papers III and IV). It is for these reasons that for practical considerations, most experiments in this thesis use DIC to first build NVNs, and then use fluorescence to record images for further analysis.

The resolution of the optical microscope is limited by the diffraction of the light. The limit is approximately equal to half of the excitation light wavelength, so objects with critical dimensions smaller than this, including lipid membrane nanotube diameter, cannot be measured directly. There are several modern super resolution microscopy techniques which can capture images with much higher resolution. Application of these techniques for sizing lipid nanotubes is complicated by the fact that the nanotube is suspended in solution between two vesicles, and is fluctuating in position on the micrometer scale. Stimulated emission depletion (STED) microscopy was chosen among the other super resolution techniques for its fast frame acquisition time to minimize image blur and validate the nanotube radii measurements (Paper IV). This chapter will provide more details on DIC, fluorescence and STED microscopy.

5.1. Differential interference contrast microscopy

DIC microscopy [130] enhances contrast by converting the information about optical path length gradients across the transparent sample into visible change in brightness. The
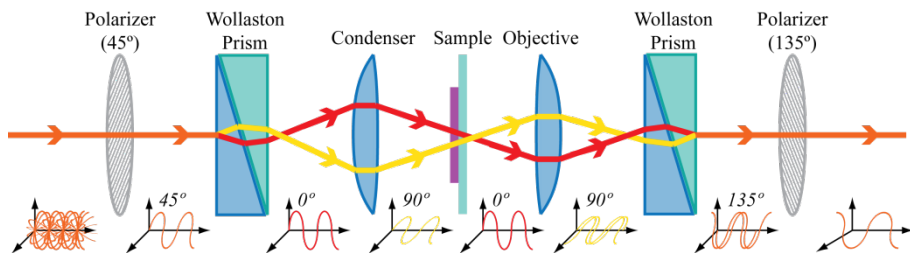
Figure 5.1 Illustration of the optical train as light passes through the DIC microscope. Two rays with 0° and 90° polarization are shown with red and yellow lines, respectively.

main components and light pass through the DIC microscope are illustrated in Figure 5.1. Before reaching the sample, light from the source is polarized at 45° and sent through Nomarski-modified Wollaston prism. The beam is split into 0° and 90° polarized rays by the prism. The condenser then focuses the two rays so that they pass through the sample offset by around 200nm. When the slightly separated rays travel through areas with thickness or refractive index gradients their optical path lengths and phases become different. After exiting the sample, the light is collected by the objective and again directed to the Nomarski-modified Wollaston prisms, where the two rays are combined back to one with 135° polarization. Because of the phase difference induced by sample and offset of the two rays, the image obtained by aligning and interference of the two rays contains dark and light shadows, which correspond to steep gradients in sample thickness or optical properties.

5.2. Wide-field laser-induced fluorescence microscopy

Wide-field or epifluorescence microscopes are widely used to image specimens labeled with fluorescent dyes [130]. Figure 5.2 shows the main components of the wide-field microscopy setup, using a laser as a source of monochromatic light. The beam produced by the laser is expanded in diameter by the telescope, consisting of the two lenses, then it is focused to be reflected by dichroic mirror and to pass through the objective. The beam is aligned in such manner that it homogeneously illuminates the field of view. The wavelength of the laser was matched to the chosen dye to allow the photon absorption to cause an electron in the dye molecule to switch from ground (S_0) to excited (S_1) energy state and then emit a photon of longer wavelength. The process of emitting the photon is called fluorescence, and it happens in a time period on the order of nanoseconds.

The difference in energy between the absorbed and emitted photon is called the Stokes' shift and is due to the existence of several vibrational energy levels with extremely short
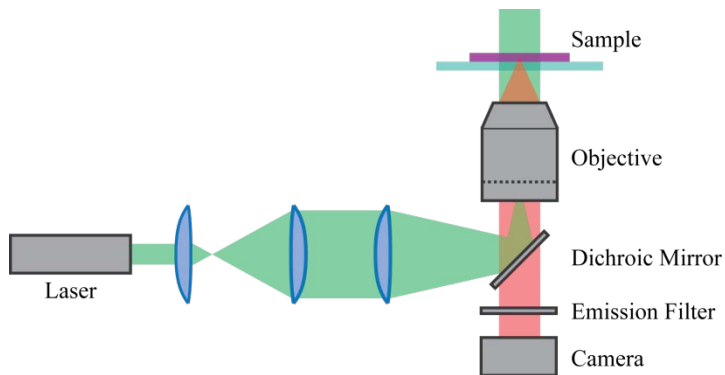
Figure 5.2 Illustration of a wide-field laser-induced fluorescence microscopy setup. The illumination light is shown in green, and the emitted light, collected by the objective, is shown in red.

lifetimes (~picoseconds) within both S_0 and S_1 states. Electrons are usually excited from the lowest level of the S_0 state. After excitation to the S_1 state, they relax to the lower vibrational levels, before emitting a photon, and after they return to the ground state they relax to lower vibrational levels again. The Stokes' shift cost by partial energy conversion to heat, enables the separation of the much weaker emitted signal, collected through the objective, from the illumination light, using a dichroic mirror and emission filter (Figure 5.2).

Excited fluorophores emit light in all directions, and only a fraction is collected by the objective (Figure 5.3). The light gathering ability of the objective is characterized by its numerical aperture (NA) [131]

$$NA = \text{n} \cdot \sin(\theta)$$

(5.1)

where θ is the half-angle of the largest cone of light which enters the objective and n is the refractive index of the medium between specimen and objective lens ($n = 1$ for air and can be ~1.5 for immersion oils).

The objective also defines the magnification and resolution of the image. The resolution (R) is limited by the fact that each point source of fluorescence is represented at the image by its diffraction pattern. This sets the minimal distance between points of the specimen at which they still can be distinguished [131]

$$R = \frac{\lambda}{2NA}$$

(5.2)

where λ is the wavelength of the illumination light.

A   **B**
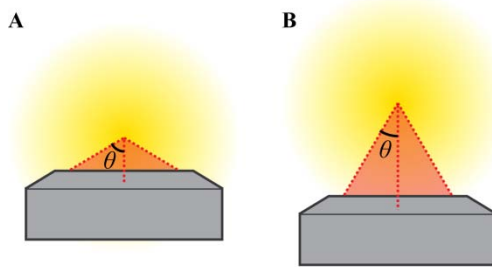
Figure 5.3 Light gathering by high (A) and low (B) NA objectives.

Another important parameter of the imaging is axial resolution or depth of field (DOF). DOF is the distance between the nearest and farthest plane of the specimen which simultaneously appear in focus. The DOF value determines the thickness of the optical sections and is given by [131]

$$DOF = \frac{\lambda n}{NA^2} + \left(\frac{n}{M} \cdot NA\right) e \qquad (5.3)$$

where *M* is the objective magnification and *e* is the smallest distance that can be resolved by a detector, placed in the objective image plane. The DOF depends strongly on objective NA, for example, when two air 40x objectives with 0.75 and 0.55 NAs are compared using $\lambda = 530$nm and $e = 11\mu$m, the DOF almost doubles from 1.1 to 1.9µm with the decrease in NA.

5.3. Confocal laser scanning microscopy

Wide-field illumination, used in traditional fluorescence microscopes, is an imaging technique which leads to excitation of the fluorophores in both the imaging plane and along the entire optical path through the specimen. As a result, the detected fluorescence can contain a significant fraction from out-of-focus fluorophores in parts of the sample. In contrast, confocal microscopy [130] is the scanning micrograph technique. The illumination laser beam (Figure 5.4, green) is focused by the objective to a very small spot (typically diffraction limited), so that only a small volume of the sample is excited. The produced fluorescence signal is gathered by the objective and separated from reflected and scattered light in the same manner as during wide-field imaging. An additional component is placed at the conjugate imaging plane, en route to the detector, known as a pinhole or aperture. This element acts as a lateral spatial filter, and prevents most out-of-focus light (Figure 5.4, dotted red lines) from reaching the detector. In this manner, only light emitted very close to the focal plane (Figure 5.4, solid red lines) can be detected.
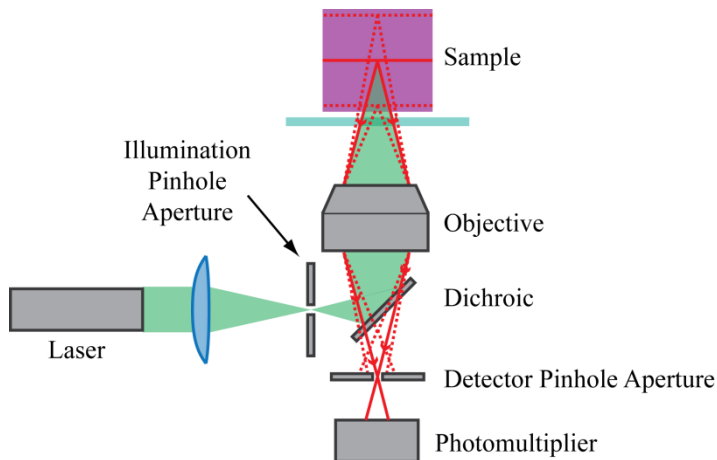
Figure 5.4 Schematic illustration of a laser scanning confocal microscope. The excitation beam is shown in green. The fluorescent signal from focal plane (solid red lines) passes through the detector pinhole aperture, while signals from lower and upper sections of the sample (dotted red lines) are blocked.

To form two-dimensional images, the area of the interest is scanned with the beam and the signal from each spot is recorded as intensity on a point detector (typically a photomultiplier tube, PMT). The use of a highly focused beam and a pinhole, gives confocal microscopy significant axial resolution improvement, and permits imaging of thin optical sections at various planes within the sample, which can be reconstructed into three-dimensional images. The lateral resolution can be only slightly improved over the limit stated in eqn. 5.2. Since the illumination volume is in fact a three-dimensional diffraction pattern, by decreasing the detector pinhole to a certain size it is possible to eliminate light from parts of the diffraction pattern of order higher than one. As a result, the lateral resolution increases slightly, however, the signal intensity is also significantly decreased, which may cause the signal to noise ratio to decrease, limiting the resolution of the confocal images.

5.4. Stimulated emission depletion microscopy

One of the modern techniques able to side-step the optical diffraction limit for lateral resolution is STED microscopy [132]. It uses two laser beams to scan through the sample. Firstly, an excitation laser pulse illuminates the sample (Figure 5.5B), producing diffraction pattern, as in confocal laser scanning microscope. The excitation pulse is immediately followed by a pulse of a doughnut-shaped beam (STED beam, Figure 5.5C, F), which
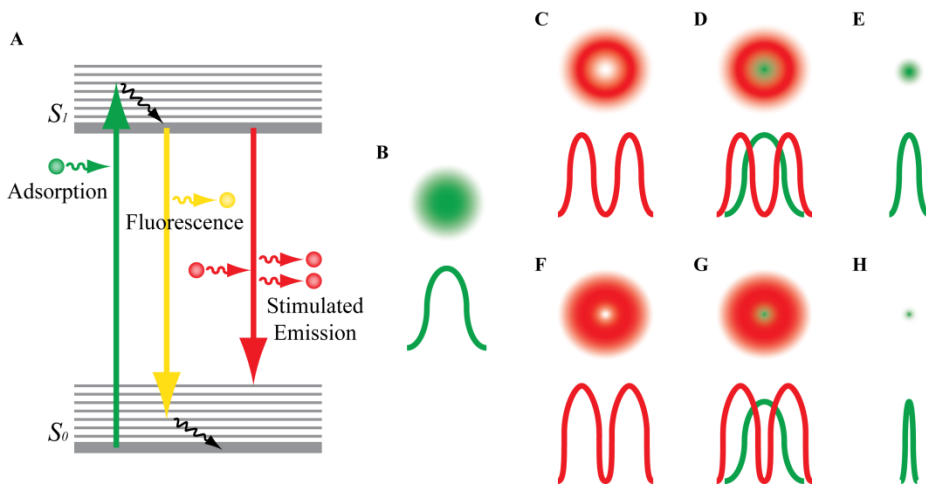
Figure 5.5 Main principles of STED microscopy. (A) Energy diagram illustrating wavelength shift for absorption, fluorescence and stimulated emission. (B-H) Schematic beam profiles for excitation (B) and STED (C and F) pulses with different maximum intensity, their disposition (D and G) and resulting effective excitation spot (E and H).

prevents fluorescence from the outer part of the excited spot, inducing the phenomena called stimulated emission. In contrast to spontaneous emission (fluorescence, Figure 5.5A, yellow), in the process of stimulated emission (Figure 5.5A, red) the electron in its excited state may return to a ground state under the influence of light of a certain wavelength. The wavelength of a STED beam and light produced by stimulated emission are shifted to the red part of the spectra (Figure 5.5A) and can be filtered out from the final signal.

The effectiveness of the stimulated emission depends on the intensity of the stimulation beam. The value of the intensity at which the probability of fluorescence emission is reduced by half is called the effective saturation intensity (I_S). The intensity maximum of the STED pulse (I_{STED}) is so high that all fluorescence is depleted, while intensity at the center of the doughnut is still low enough that fluorophores there are unaffected and are able to emit fluorescence. The effective size of the scanning spot (Figure5.5E, H) is narrower and results in new improved resolution (R) [133]

$$R = \frac{\lambda}{2NA\sqrt{1 + \frac{I_{STED}}{I_S}}}$$

(5.4)

which is limited only by I_{STED} and photodegradation of the sample. The gain in resolution with increase of the I_{STED} is illustrated by the Figure 5.5 C-E versus F-H. The typical lateral resolutions achieved by STED microscopy are 20-90nm.

6 SUMMARY OF PAPERS

Paper I: Spontaneous Shape Transformation of Free-Floating Lipid Membrane Nanotubes

Extremely long linear lipid membrane nanotubes can be prepared from MLV-GUV complexes and then released by electrofission (Figure 6.1A-B). After release, this high energy curved structure is no longer stable and undergoes shape transformation to minimize its curvature energy. Paper I considers two alternative transformation mechanisms, swelling and folding. Quantitative fluorescence intensity analysis and examination of the membrane permeability properties highlight that the swelling mechanism is highly unfavorable. Moreover, experiments performed with different membrane dye have demonstrated that the process dynamics can be changed by the choice of label, and revealed evidence supporting the folding mechanism for the transformation.

During the folding transformation of a nanotube, one or several double walled stomatocyte-like pockets appear along its length (Figure 6.1C-F) and then continue to elongate consuming nanotube membrane. By this mechanism the curvature can relax
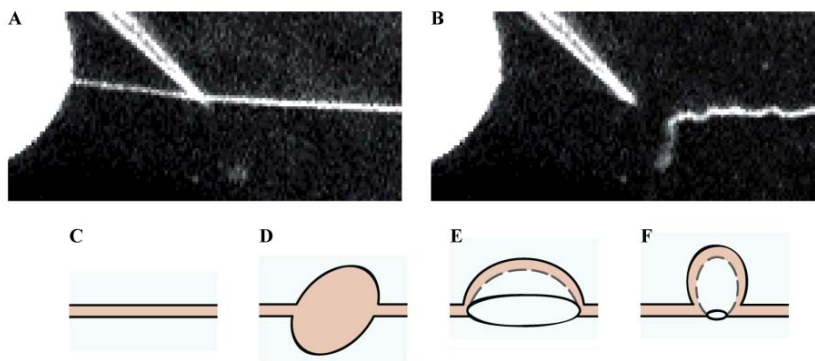
Figure 6.1 Release and transformation of lipid membrane nanotubes. (A-B) Fluorescent images showing electrofission of the nanotube end from a vesicle membrane. (C-D) Schematic illustrations of the key steps of the folding transformation mechanism. Firstly, the discocyte (D) forms on the original nanotube (C). It then folds (E), closing into stomatocyte-like structure (F). The inner volume of the structure is marked with red.

without solution flowing through the membrane, which would be required for swelling. In the same time, the nanotube membrane experiences high rates of the interleaflet lipid transfer ($\sim$0.01-0.001s^{-1}) necessary to decrease initial several square micrometers area difference between outer and inner leaflets of the membrane.

Paper II: Generation of Phospholipid Vesicle-Nanotube Networks and Transport of Molecules therein

Paper II provides a detailed step-by-step protocol for the preparation of surface-immobilized NVNs, supporting both analyte and nanoparticle transport. The construction procedure gives unique control over the network topology and content of the individual containers. The networks are stable over period of several hours and are useful for performing biomimetic experiments.

This paper describes three modes of transport driven by tension, electric field and passive diffusion, an example of which is highlighted in Figure 6.2. Passive transport by diffusion does not require any additional manipulations with the network. The other two modes are active transport modes which can be switched on and off. The electric field driven transport requires insertion of two specially prepared microelectrodes into the network. The tension driven transport is most commonly induced by physical deformation of one vesicle in the network by a glass micropipette.
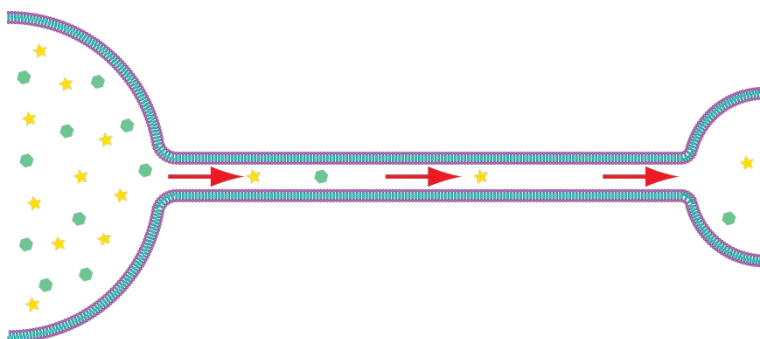
Figure 6.2 Schematic illustration of the minimal network for the transport experiments. The concentration gradient is formed by the injection of different solution into each vesicle.

Paper III: Radial Sizing of Lipid Nanotubes Using Membrane Displacement Analysis

Paper III suggests a method for the determination of lipid nanotube radii, based on the measurement of membrane material flow from the MLV through the GUV's and nanotube's surface to a developing DV volume. This flow can be visualized by photobleaching a section of the nanotube and following its translocation. The DV radius and coordinate of the bleached region are determined from recorded image series (Figure 6.3A) and used to calculate the nanotube radius from the surface area conservation law. Our estimations suggest that if the method is applied correctly, the surface tension induced by the DV inflation is insufficient to affect nanotube radii. The method was demonstrated to work for both artificial lipid membranes and for cell plasma membrane blebs.

Studies of nanotubes pulled from population of vesicles result in multiple peak distributions for measured radii values. An example of such a distribution is shown in Figure 6.3B. Each peak corresponds to a different lamellarity of the GUV and the nanotube, where the measured values are the distances between the nanotube center and the midpoint of the nanotube wall. The method sensitivity to the number of the bilayers in the nanotube wall helped to unify and explain variation in values previously found by tether coalescence and the electrochemical approach, and moreover, provides a tool to not only investigate nanotube size, but also inspect the lamellarity of the model systems.
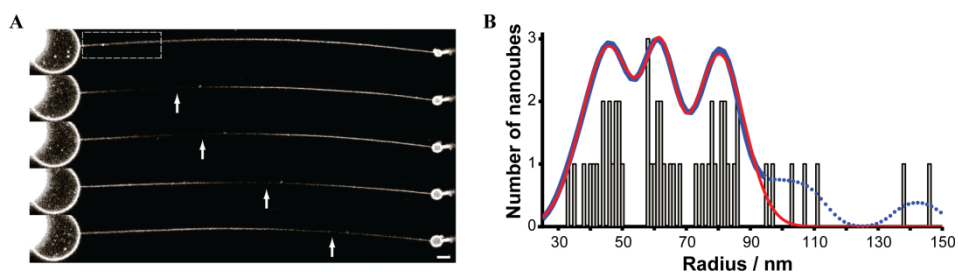
Figure 6.3 Nanotube radius determination using membrane displacement analysis. (A) Typical confocal series, recoded for single measurement, illustrating the visible growth of the DV radius and movement of the bleached region (white arrows) along the nanotube. Scale bar represents 10µm. (B) Distribution of the measured nanotube radii (n = 50) for SPE membrane with addition of 5mol% cholesterol.

Paper IV: Studying compositional and environmental effects on the bending rigidity of vesicles and cell plasma membranes using lipid nanotubes

Bending rigidity of lipid membranes is sensitive to all factors affecting organization and packing of the lipid molecules in the bilayer. These effects can be studied by means of the nanotube radii measurement scheme described in Paper III, due to the direct connection between nanotube radius and membrane rigidity, in systems where surface tension is buffered by the presence of a membrane reservoir.

Paper IV proves sensitivity of the membrane displacement radial sizing technique to changes in the membrane composition, using lipid mixtures containing various sterols (cholesterol, lathosterol, sitosterol, 7-dehydrocholesterol and lanosterol), and to environmental changes, through variances in concentration of the sodium ions in solution (Figure 6.4). The addition of 100mM sodium chloride to experimental buffer results in a huge increase in the radius of the unilamellar nanotubes (from 56 to 100nm). This allows us to validate the radii measurement technique with STED super resolution microscopy, whose resolution would still commonly be unable to distinguish radii changes. The radii derived from the STED images were in agreement with the results of the membrane displacement analysis method.

It was also demonstrated that it is possible to investigate the bending rigidity of the cell plasma membrane. For example, the plasma membrane of NG108-15 cells loses 40% of its rigidity after 30min treatment with MβCD, depleting the membrane of cholesterol.
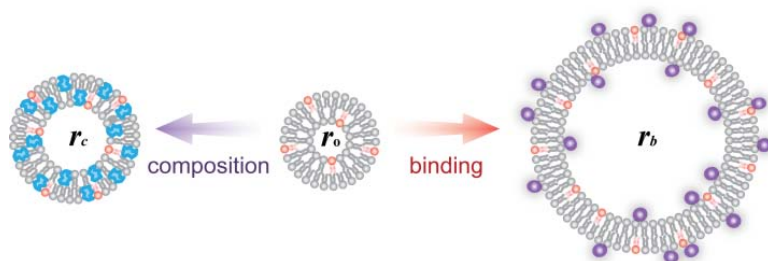
Figure 6.4 The bending rigidity of the membranes can be affected by varying the membrane composition or by membrane interactions with soluble molecules in the local environment. Its alterations affect the equilibrium radius of produced nanotubes, which can be monitored using membrane displacement analysis.

Paper V: A Microfluidic Pipette for Single-Cell Pharmacology

Paper V presents a free-standing device named a microfluidic pipette, which is able to create a stable open volume of recirculating solution. The volume is self-confined, and the solution in it does not mix with surrounding liquid. The recirculation volume is formed when laminar fluid stream exiting from middle channel are fully recaptured by two neighboring channels (Figure 6.5B), and can be as small as 10µm. The pipette is build out of soft material and can be connected with a flow-switching device, so that it is capable of both fast solution exchange as well as dilutions.

The microfluidic pipette is a helpful tool for single cell studies, as it can deliver solutions to a selected group of intact adherent cells without contaminating the surrounding solution (Figure 6.5A). This has been used to selectively induce cell plasma membrane blebs formation (Figure 6.5C-E) and to activate ion channels by delivering an agonist solution to a specific cell simultaneously with patch-clamp measurements.
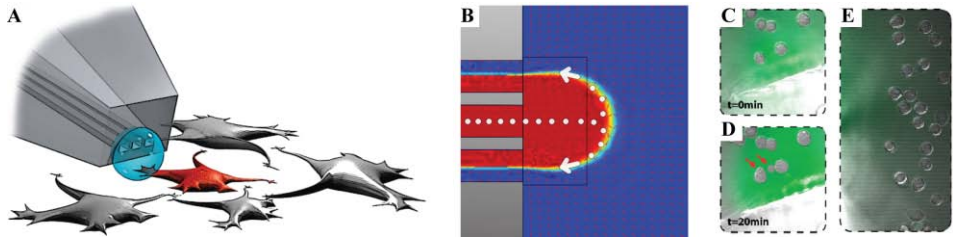
Figure 6.5 The microfluidic pipette is capable of selective exposure of a single cell to selected solutions without contaminating the rest of the volume (A). The solution exits from middle channel and is then fully recaptured into two neighboring channels, creating a recirculation volume with stationary concentration pattern (B). The microfluidic pipette can be used to induce formation of the plasma membrane blebs on selected group of cells. The cells inside the recirculation zone (C) produce blebs after 20min exposure to blebbing solution (D), but the cells outside the recirculation zone (E) remain unaffected. (C-E) are 75µm wide.

7 CONCLUDING REMARKS

In biological cells a great number of events take place simultaneously to fulfill all the cell functions. The behavior of cellular membranes is governed by complex relationships between lipids and proteins which have significant interplay, affecting membrane shapes and respective functions. To study such a system as a whole is extremely complicated, and therefore, in order to gain understanding of these complex systems, they are typically broken into key parts. Lipid bilayer properties have been examined using various artificial membrane models, but further studies are required to fully understand the pivotal role of these structures.

This thesis explores the advantages offered by NVN's in the investigation of the dynamic processes occurring at nanoscale within these membrane structures. Analysis of the transformation of lipid membrane nanotubes gives an insight into the influence of the basic membrane properties on the dynamics and the transformation path to the final shape. These experiments also reveal that a fluorescent label can have a noticeable effect on membrane dynamics. Studies of the transport through tiny nanotube opening, in particular, diffusion- and tension-driven modes, can help us understand cell communication via intercellular nanotubes.

A significant advance has been made in the characterization of the NVNs, by introducing a convenient method for nanotube radial sizing. Nanotube radius is a key parameter and is essential for the interpretation of all experiments performed with the NVNs. The radial sizing method is also capable of evaluating the lamellarity distribution in the GUV population and can potentially be used to control and optimize the MLV-GUV complex preparation protocol. Moreover, the method is useful for the study of membrane bending rigidity dependence on the membrane composition and local environment. In perspective it can be used together with the microfluidic pipette, for probing the bending rigidity of plasma membranes from a selected cell without affecting the rest of the culture. The microfluidic pipette by itself is an extremely convenient and powerful tool which is currently being developed.

Future work with NVNs should be directed towards the inclusion of more dynamic cellular mechanisms by introducing protein components into the system. This can be achieved by utilizing cell plasma membrane blebs or by selective exposure of the NVN or its constituents, to a solution of the membrane remodeling proteins using the microfluidic pipette.

8 ACKNOWLEDGMENTS

This thesis would not have been possible without the support of many people.

I would like to express my gratitude to my supervisors:

Professor Owe Orwar, for giving me the wonderful opportunity to be a part your group and participate in several interesting projects.

Professor Gavin Jeffries, for your guidance and advice, a lot of help, and being a great company in the adventurous "European super resolution microscopy tour".

I am very grateful to all coauthors of the papers in this thesis and to past and present members of the group.

I would like to give my special thanks to following people:

To Ilona, Celine, Anna and Kiryl for your friendship, support and a lot of good times. I hope, that even though most of us are going to leave Göteborg, we will still find opportunities to meet in the future.

To my great officemates Shijun and Akram.

To all my friends outside the group, especially Катя & Nils, Оля, Сережа, Даша, Лиза, Женя и Виталик.

To my husband Andre, for your love, care, support and patience.

9 REFERENCES

1. Alberts, B., *Molecular biology of the cell*. 5th ed. 2008, New York: Garland Science. 1 v. (various pages).

2. Levental, I., M. Grzybek, and K. Simons, *Greasing their way: lipid modifications determine protein association with membrane rafts*. Biochemistry, 2010. **49**(30): p. 6305-6316.

3. Westermann, B., *Mitochondrial fusion and fission in cell life and death*. Nat. Rev. Mol. Cell Biol., 2010. **11**(12): p. 872-884.

4. Klumperman, J., *Architecture of the mammalian Golgi*. Cold Spring Harb Perspect. Biol., 2011. **3**(7): p. a005181.

5. Appenzeller-Herzog, C. and H.P. Hauri, *The ER-Golgi intermediate compartment (ERGIC): in search of its identity and function*. J. Cell Sci., 2006. **119**(Pt 11): p. 2173-2183.

6. Jahn, R. and D. Fasshauer, *Molecular machines governing exocytosis of synaptic vesicles*. Nature, 2012. **490**(7419): p. 201-207.

7. Gerdes, H.H., N.V. Bukoreshtliev, and J.F. Barroso, *Tunneling nanotubes: a new route for the exchange of components between animal cells*. FEBS Lett., 2007. **581**(11): p. 2194-2201.

8. Tamm, L.K., J. Crane, and V. Kiessling, *Membrane fusion: a structural perspective on the interplay of lipids and proteins*. Curr. Opin. Struct. Biol., 2003. **13**(4): p. 453-466.

9. Walde, P., et al., *Giant vesicles: preparations and applications*. ChemBioChem, 2010. **11**(7): p. 848-865.

10. Sackmann, E., *Supported membranes: scientific and practical applications*. Science, 1996. **271**(5245): p. 43-48.

11. Karlsson, M., et al., *Electroinjection of colloid particles and biopolymers into single unilamellar liposomes and cells for bioanalytical applications*. Anal. Chem., 2000. **72**(23): p. 5857-5862.

12. Lobovkina, T., et al., *Shape optimization in lipid nanotube networks*. Eur. Phys. J. E Soft Matter, 2008. **26**(3): p. 295-300.

13. Lobovkina, T., et al., *Zipper dynamics of surfactant nanotube Y junctions*. Phys. Rev. Lett., 2006. **97**(18): p. 188105.

14. Lobovkina, T., et al., *Mechanical tweezer action by self-tightening knots in surfactant nanotubes*. Proc. Natl. Acad. Sci. USA, 2004. **101**(21): p. 7949-7953.

15. Cans, A.S., et al., *Artificial cells: unique insights into exocytosis using liposomes and lipid nanotubes*. Proc. Natl. Acad. Sci. USA, 2003. **100**(2): p. 400-404.

16. Bar-Ziv, R., E. Moses, and P. Nelson, *Dynamic excitations in membranes induced by optical tweezers.* Biophys. J., 1998. **75**(1): p. 294-320.

17. Hotani, H., *Transformation pathways of liposomes.* J. Mol. Biol., 1984. **178**(1): p. 113-120.

18. Majhenc, J., et al., *Phospholipid membrane bending as assessed by the shape sequence of giant oblate phospholipid vesicles.* Biochim. Biophys. Acta, 2004. **1664**(2): p. 257-266.

19. Lobovkina, T., et al., *Formation and release of circular lipid nanotubes.* Soft Matter, 2008. **4**(3): p. 467-470.

20. Raphael, R.M. and R.E. Waugh, *Accelerated interleaflet transport of phosphatidylcholine molecules in membranes under deformation.* Biophys. J., 1996. **71**(3): p. 1374-1388.

21. Hurtig, J., D.T. Chiu, and B. Onfelt, *Intercellular nanotubes: insights from imaging studies and beyond.* Wiley Interdiscip. Rev. Nanomed. Nanobiotechnol., 2010. **2**(3): p. 260-276.

22. Lizana, L., B. Bauer, and O. Orwar, *Controlling the rates of biochemical reactions and signaling networks by shape and volume changes.* Proc. Natl. Acad. Sci. USA, 2008. **105**(11): p. 4099-4104.

23. Sott, K., et al., *Controlling enzymatic reactions by geometry in a biomimetic nanoscale network.* Nano Lett., 2006. **6**(2): p. 209-214.

24. Tokarz, M., et al., *Electrophoretic transport of latex particles in lipid nanotubes.* Langmuir, 2007. **23**(14): p. 7652-7658.

25. Adams, K.L., et al., *Steady-state electrochemical determination of lipidic nanotube diameter utilizing an artificial cell model.* Anal. Chem., 2010. **82**(3): p. 1020-1026.

26. Zhu, D., et al., *Hydrogen peroxide alters membrane and cytoskeleton properties and increases intercellular connections in astrocytes.* J. Cell Sci., 2005. **118**(Pt 16): p. 3695-3703.

27. Gondre-Lewis, M.C., et al., *Abnormal sterols in cholesterol-deficiency diseases cause secretory granule malformation and decreased membrane curvature.* J. Cell Sci., 2006. **119**(Pt 9): p. 1876-1885.

28. McMahon, H.T. and J.L. Gallop, *Membrane curvature and mechanisms of dynamic cell membrane remodelling.* Nature, 2005. **438**(7068): p. 590-596.

29. Scott, R.E., *Plasma membrane vesiculation: a new technique for isolation of plasma membranes.* Science, 1976. **194**(4266): p. 743-745.

30. Bauer, B., M. Davidson, and O. Orwar, *Proteomic analysis of plasma membrane vesicles.* Angew. Chem. Int. Ed. (English), 2009. **48**(9): p. 1656-1659.

31. Baumann, N.A., et al., *Cell surface display and intracellular trafficking of free glycosylphosphatidylinositols in mammalian cells.* J. Biol. Chem., 2000. **275**(10): p. 7378-7389.

32. Holowka, D. and B. Baird, *Lactoperoxidase-catalyzed iodination of the receptor for immunoglobulin E at the cytoplasmic side of the plasma membrane.* J. Biol. Chem., 1984. **259**(6): p. 3720-3728.

33. Bauer, B., M. Davidson, and O. Orwar, *Direct reconstitution of plasma membrane lipids and proteins in nanotube-vesicle networks.* Langmuir, 2006. **22**(22): p. 9329-9332.

34. Finkelstein, A., *Lipid bilayer membranes: their permeability properties as related to those of cell membranes*, in *Physiology of Membrane Disorders*, T. Andreoli, J. Hoffman, and D. Fanestil, Editors. 1978, Springer US. p. 205-216.

35. Almeida, P.F.F. and W.L.C. Vaz, *Chapter 6 Lateral diffusion in membranes*, in *Handbook of Biological Physics*, R. Lipowsky and E. Sackmann, Editors. 1995, North-Holland. p. 305-357.

36. Contreras, F.X., et al., *Transbilayer (flip-flop) lipid motion and lipid scrambling in membranes.* FEBS Lett., 2010. **584**(9): p. 1779-1786.

37. Bagatolli, L. and P.B.S. Kumar, *Phase behavior of multicomponent membranes: experimental and computational techniques.* Soft Matter, 2009. **5**(17): p. 3234-3248.

38. Ries, R.S., et al., *Black lipid membranes: visualizing the structure, dynamics, and substrate dependence of membranes.* J. Phys. Chem. B, 2004. **108**(41): p. 16040-16049.

39. Israelachvili, J.N., S. Marcelja, and R.G. Horn, *Physical principles of membrane organization.* Q. Rev. Biophys., 1980. **13**(2): p. 121-200.

40. Heinrich, M., et al., *Dynamic sorting of lipids and proteins in membrane tubes with a moving phase boundary.* Proc. Natl. Acad. Sci. USA, 2010. **107**(16): p. 7208-7213.

41. Reimhult, E., F. Hook, and B. Kasemo, *Intact vesicle adsorption and supported biomembrane formation from vesicles in solution: influence of surface chemistry, vesicle size, temperature, and osmotic pressure.* Langmuir, 2003. **19**(5): p. 1681-1691.

42. Lasic, D.D., *Liposomes: from physics to applications*. 1993, Amsterdam ; New York: Elsevier. xviii, 575 p.

43. Evans, E. and D. Needham, *Physical-properties of surfactant bilayer-membranes - thermal transitions, elasticity, rigidity, cohesion, and colloidal interactions.* J. Phys. Chem., 1987. **91**(16): p. 4219-4228.

44. Rossier, O., et al., *Giant vesicles under flows: extrusion and retraction of tubes.* Langmuir, 2003. **19**(3): p. 575-584.

45. Zhou, H.N., et al., *Stretching and relaxation of vesicles.* Phys. Rev. E, 2011. **83**(1): p. 011905.

46. Onoue, Y., et al., *A giant liposome for single-molecule observation of conformational changes in membrane proteins.* Biochim. Biophys. Acta-Biomembranes, 2009. **1788**(6): p. 1332-1340.

47. Girard, P., et al., *A new method for the reconstitution of membrane proteins into giant unilamellar vesicles.* Biophys. J., 2004. **87**(1): p. 419-429.

48. Kahya, N., *Light on fluorescent lipids in rafts: a lesson from model membranes.* Biochem. J., 2010. **430**(3): p. e7-e9.

49. Roux, A., et al., *A minimal system allowing tubulation with molecular motors pulling on giant liposomes.* Proc. Natl. Acad. Sci. USA, 2002. **99**(8): p. 5394-5399.

50. Akashi, K., et al., *Preparation of giant liposomes in physiological conditions and their characterization under an optical microscope.* Biophys. J., 1996. **71**(6): p. 3242-3250.

51. Pott, T., H. Bouvrais, and P. Meleard, *Giant unilamellar vesicle formation under physiologically relevant conditions.* Chem. Phys. Lipids, 2008. **154**(2): p. 115-119.

52. Estes, D.J. and M. Mayer, *Giant liposomes in physiological buffer using electroformation in a flow chamber.* Biochim. Biophys. Acta, 2005. **1712**(2): p. 152-160.

53. Ota, S., S. Yoshizawa, and S. Takeuchi, *Microfluidic formation of monodisperse, cell-sized, and unilamellar vesicles.* Angew. Chem. Int. Ed. (English), 2009. **48**(35): p. 6533-6537.

54. Billerit, C., et al., *Formation of giant unilamellar vesicles from spin-coated lipid films by localized IR heating.* Soft Matter, 2012. **8**(42): p. 10823-10826.

55. Criado, M. and B.U. Keller, *A membrane-fusion strategy for single-channel recordings of membranes usually non-accessible to patch-clamppipette electrodes.* FEBS Lett., 1987. **224**(1): p. 172-176.

56. Karlsson, M., et al., *Micropipet-assisted formation of microscopic networks of unilamellar lipid bilayer nanotubes and containers.* Langmuir, 2001. **17**(22): p. 6754-6758.

57. Billerit, C., et al., *Heat-induced formation of single giant unilamellar vesicles.* Soft Matter, 2011. **7**(20): p. 9751-9757.

58. Sawant, R.R. and V.P. Torchilin, *Liposomes as 'smart' pharmaceutical nanocarriers.* Soft Matter, 2010. **6**(17): p. 4026-4044.

59. Gruber, H.J. and H. Schindler, *External surface and lamellarity of lipid vesicles: a practice-oriented set of assay methods.* Biochim. Biophys. Acta, 1994. **1189**(2): p. 212-224.

60.   Kwok, R. and E. Evans, *Thermoelasticity of large lecithin bilayer vesicles.* Biophys. J., 1981. **35**(3): p. 637-652.

61.   Akashi, K., et al., *Preparation of giant liposomes in physiological conditions and their characterization under an optical microscope.* Biophys J, 1996. **71**(6): p. 3242-3250.

62.   Sackmann, E., *Chapter 1 Biological membranes architecture and function*, in *Handbook of Biological Physics*, R. Lipowsky and E. Sackmann, Editors. 1995, North-Holland. p. 1-63.

63.   Lipowsky, R., *The conformation of membranes.* Nature, 1991. **349**(6309): p. 475-481.

64.   Seifert, U. and R. Lepowsky, *Chapter 8 Morphology of vesicles*, in *Handbook of Biological Physics*, R. Lipowsky and E. Sackmann, Editors. 1995, North-Holland. p. 403-463.

65.   Friedl, P. and K. Wolf, *Tumour-cell invasion and migration: diversity and escape mechanisms.* Nat. Rev. Cancer, 2003. **3**(5): p. 362-374.

66.   Boucrot, E. and T. Kirchhausen, *Endosomal recycling controls plasma membrane area during mitosis.* Proc. Natl. Acad. Sci. USA, 2007. **104**(19): p. 7939-7944.

67.   Mills, J.C., et al., *Apoptotic membrane blebbing is regulated by myosin light chain phosphorylation.* J. Cell. Biol., 1998. **140**(3): p. 627-636.

68.   Charras, G.T., et al., *Life and times of a cellular bleb.* Biophys. J., 2008. **94**(5): p. 1836-1853.

69.   Scott, R.E., *Plasma membrane vesiculation: a new technique for isolation of plasma membranes.* Science, 1976. **194**(4266): p. 743-745.

70.   Scott, R.E., et al., *Plasma membrane vesiculation in 3T3 and SV3T3 cells.* J. Cell Sci., 1979. **35**: p. 229-243.

71.   Arriaga, E.A., *Single cell heterogeneity*, in *Single Cell Analysis*. 2009, Wiley-VCH Verlag GmbH & Co. KGaA. p. 223-234.

72.   Brehm-Stecher, B.F. and E.A. Johnson, *Single-cell microbiology: tools, technologies, and applications.* Microbiol. Mol. Biol. Rev., 2004. **68**(3): p. 538-559.

73.   Whitesides, G.M., *The origins and the future of microfluidics.* Nature, 2006. **442**(7101): p. 368-373.

74.   Yin, H. and D. Marshall, *Microfluidics for single cell analysis.* Curr. Opin. Biotechnol., 2012. **23**(1): p. 110-119.

75.   Dunlop, J., et al., *High-throughput electrophysiology: an emerging paradigm for ion-channel screening and physiology.* Nat. Rev. Drug Discov., 2008. **7**(4): p. 358-368.

76.   Zhang, H. and K.K. Liu, *Optical tweezers for single cells.* J. R. Soc. Interface, 2008. **5**(24): p. 671-690.

77.   Sengupta, P., S. Van Engelenburg, and J. Lippincott-Schwartz, *Visualizing cell structure and function with point-localization superresolution imaging.* Dev. Cell, 2012. **23**(6): p. 1092-1102.

78.   Jansson, E.T., et al., *Microfluidic flow cell for sequential digestion of immobilized proteoliposomes.* Anal. Chem., 2012. **84**(13): p. 5582-5588.

79.   Lanigan, P.M.P., et al., *A microfluidic platform for probing single cell plasma membranes using optically trapped Smart Droplet Microtools (SDMs).* Lab Chip, 2009. **9**(8): p. 1096-1101.

80.   Evans, E. and W. Rawicz, *Entropy-driven tension and bending elasticity in condensed-fluid membranes.* Phys. Rev. Lett., 1990. **64**(17): p. 2094-2097.

81.   Needham, D. and R.S. Nunn, *Elastic deformation and failure of lipid bilayer membranes containing cholesterol.* Biophys. J., 1990. **58**(4): p. 997-1009.

82.   Zhelev, D.V., *Material property characteristics for lipid bilayers containing lysolipid.* Biophys. J., 1998. **75**(1): p. 321-330.

83.   Koenig, B.W., H.H. Strey, and K. Gawrisch, *Membrane lateral compressibility determined by NMR and x-ray diffraction: effect of acyl chain polyunsaturation.* Biophys. J., 1997. **73**(4): p. 1954-1966.

84.   Olbrich, K., et al., *Water permeability and mechanical strength of polyunsaturated lipid bilayers.* Biophys. J., 2000. **79**(1): p. 321-327.

85.   Brochard, F. and J.F. Lennon, *Frequency spectrum of the flicker phenomenon in erythrocytes.* Journal de Physique, 1975. **36**(11): p. 1035-1047.

86.   Nagle, J.F., *Introductory lecture: basic quantities in model biomembranes.* Farad. Discuss., 2013. **161**(0): p. 11-29.

87.   Böckmann, R.A., et al., *Effect of sodium chloride on a lipid bilayer.* Biophys. J., 2003. **85**(3): p. 1647-1655.

88.   Rao, M., et al., *Depletion of cellular cholesterol interferes with intracellular trafficking of liposome-encapsulated ovalbumin.* Immunol. Cell Biol., 2003. **81**(6): p. 415-423.

89.   Rodal, S.K., et al., *Extraction of cholesterol with methyl-beta-cyclodextrin perturbs formation of clathrin-coated endocytic vesicles.* Mol. Biol. Cell, 1999. **10**(4): p. 961-974.

90.   Oradd, G., V. Shahedi, and G. Lindblom, *Effect of sterol structure on the bending rigidity of lipid membranes: a (2)H NMR transverse relaxation study.* Biochim. Biophys. Acta, 2009. **1788**(9): p. 1762-1771.

91.   Deuling, H.J. and W. Helfrich, *The curvature elasticity of fluid membranes: a catalogue of vesicle shapes.* Journal de Physique, 1976. **37**: p. 1335-1345.

92.   Miao, L., et al., *Equilibrium budding and vesiculation in the curvature model of fluid lipid vesicles.* Phys. Rev. A, 1991. **43**(12): p. 6843-6856.

93.   Miao, L., et al., *Budding transitions of fluid-bilayer vesicles: the effect of area-difference elasticity.* Phys. Rev. E Stat. Phys. Plasmas Fluids Relat. Interdiscip. Topics, 1994. **49**(6): p. 5389-5407.

94.   McConnell, H.M. and R.D. Kornberg, *Inside-outside transitions of phospholipids in vesicle membranes.* Biochemistry, 1971. **10**(7): p. 1111-1120.

95.   Papadopulos, A., et al., *Flippase activity detected with unlabeled lipids by shape changes of giant unilamellar vesicles.* J. Biol. Chem., 2007. **282**(21): p. 15559-15568.

96.   Gurtovenko, A.A. and I. Vattulainen, *Molecular mechanism for lipid flip-flops.* J. Phys. Chem. B, 2007. **111**(48): p. 13554-13559.

97.   Paula, S., et al., *Permeation of protons, potassium ions, and small polar molecules through phospholipid bilayers as a function of membrane thickness.* Biophys. J., 1996. **70**(1): p. 339-348.

98.   Kedem, O. and A. Katchalsky, *Thermodynamic analysis of the permeability of biological membranes to non-electrolytes.* Biochim. Biophys. Acta, 1958. **27**(0): p. 229-246.

99.   Sakashita, A., et al., *Three-dimensional analysis of lipid vesicle transformations.* Soft Matter, 2012. **8**(33): p. 8569-8581.

100.   Sanborn, J., et al., *Transient pearling and vesiculation of membrane tubes under osmotic gradients.* Farad. Discuss., 2013. **161**(0): p. 167-176.

101.   Olbrich, K., et al., *Water permeability and mechanical strength of polyunsaturated lipid bilayers.* Biophys. J., 2000. **79**(1): p. 321-327.

102.   Berndl, K., et al., *Shape transformations of giant vesicles: extreme sensitivity to bilayer asymmetry.* Europhys. Lett., 1990. **13**(7): p. 659-664.

103.   Tsafrir, I., et al., *Pearling instabilities of membrane tubes with anchored polymers.* Phys. Rev. Lett., 2001. **86**(6): p. 1138-1141.

104.   Yu, Y. and S. Granick, *Pearling of lipid vesicles induced by nanoparticles.* J. Am. Chem. Soc., 2009. **131**(40): p. 14158-14159.

105.   Pascoal, P., et al., *Membrane nanotubes drawn by optical tweezers transmit electrical signals between mammalian cells over long distances.* Lab Chip, 2010. **10**(17): p. 2235-2241.

106.   Neumann, E., et al., *Gene transfer into mouse lyoma cells by electroporation in high electric fields.* EMBO J., 1982. **1**(7): p. 841-845.

107.   Tsong, T.Y., *Electroporation of cell membranes.* Biophys. J., 1991. **60**(2): p. 297-306.

108. Yu, Z., et al., *Therapeutic potential of irreversible electroporation in sarcoma.* Expert Rev. Anticancer Ther., 2012. **12**(2): p. 177-184.

109. Zimmerberg, J., F.S. Cohen, and A. Finkelstein, *Fusion of phospholipid-vesicles with planar phospholipid-bilayer membranes.* J. Gen. Physiol., 1980. **75**(3): p. 241-250.

110. Evans, F., et al., *The colloidal domain: where physics, chemistry, biology, and technology meet.* 1999: Wiley-VCH.

111. Glaser, R.W., et al., *Reversible electrical breakdown of lipid bilayers: formation and evolution of pores.* Biochim. Biophys. Acta, 1988. **940**(2): p. 275-287.

112. Wilhelm, C., et al., *Kinetics of pore size during irreversible electrical breakdown of lipid bilayer membranes.* Biophys. J., 1993. **64**(1): p. 121-128.

113. Seifert, U. and R. Lipowsky, *Adhesion of vesicles.* Phys. Rev. A, 1990. **42**(8): p. 4768-4771.

114. Hochmuth, R.M., N. Mohandas, and P.L. Blackshear Jr, *Measurement of the elastic modulus for red cell membrane using a fluid mechanical technique.* Biophys. J., 1973. **13**(8): p. 747-762.

115. Roux, A., et al., *GTP-dependent twisting of dynamin implicates constriction and tension in membrane fission.* Nature, 2006. **441**(7092): p. 528-531.

116. Dai, J. and M.P. Sheetz, *Mechanical properties of neuronal growth cone membranes studied by tether formation with laser optical tweezers.* Biophys. J., 1995. **68**(3): p. 988-996.

117. Raucher, D. and M.P. Sheetz, *Characteristics of a membrane reservoir buffering membrane tension.* Biophys. J., 1999. **77**(4): p. 1992-2002.

118. Derényi, I., et al., *Membrane nanotubes*, in *Controlled Nanoscale Motion*, H. Linke and A. Månsson, Editors. 2007, Springer Berlin Heidelberg. p. 141-159.

119. Cuvelier, D., et al., *Coalescence of membrane tethers: experiments, theory, and applications.* Biophys. J., 2005. **88**(4): p. 2714-2726.

120. Heinrich, V. and R.E. Waugh, *A piconewton force transducer and its application to measurement of the bending stiffness of phospholipid membranes.* Ann. Biomed. Eng., 1996. **24**(5): p. 595-605.

121. Derenyi, I., F. Julicher, and J. Prost, *Formation and interaction of membrane tubes.* Phys. Rev. Lett., 2002. **89**(20): p. 238101.

122. Evans, E., et al., *Biomembrane templates for nanoscale conduits and networks.* Science, 1996. **273**(5277): p. 933-935.

123. Dagdug, L., et al., *Equilibration in two chambers connected by a capillary.* J. Chem. Phys., 2003. **119**(23): p. 12473-12478.

124. Hurtig, J. and O. Orwar, *Injection and transport of bacteria in nanotube-vesicle networks.* Soft Matter, 2008. **4**(7): p. 1515-1520.

125. Tokarz, M., et al., *Single-file electrophoretic transport and counting of individual DNA molecules in surfactant nanotubes.* Proc. Natl. Acad. Sci. USA, 2005. **102**(26): p. 9127-9132.

126. Hurtig, J., et al., *Electrophoretic transport in surfactant nanotube networks wired on microfabricated substrates.* Anal. Chem., 2006. **78**(15): p. 5281-5288.

127. Chizmadzhev, Y.A., et al., *Lipid flow through fusion pores connecting membranes of different tensions.* Biophys. J., 1999. **76**(6): p. 2951-2965.

128. Dommersnes, P.G., et al., *Marangoni transport in lipid nanotubes.* Europhys. Lett., 2005. **70**(2): p. 271-277.

129. Karlsson, R., A. Karlsson, and O. Orwar, *Formation and transport of nanotube-integrated vesicles in a lipid bilayer network.* J. Phys. Chem. B, 2003. **107**(40): p. 11201-11207.

130. Murphy, D.B. and M.W. Davidson, *Fundamentals of light microscopy and electronic imaging.* 2nd ed. 2013, Hoboken, N.J.: Wiley-Blackwell. xiii, 538 (various pages)

131. Spring, K.R. and M.W. Davidson, *Properties of microscope objectives.* at http://www.microscopyu.com/.

132. Hell, S.W. and J. Wichmann, *Breaking the diffraction resolution limit by stimulated emission: stimulated-emission-depletion fluorescence microscopy.* Opt. Lett., 1994. **19**(11): p. 780-782.

133. Westphal, V. and S.W. Hell, *Nanoscale resolution in the focal plane of an optical microscope.* Phys. Rev. Lett., 2005. **94**(14): p. 143903.